2021

Acoustic Detection of Developmental Dysplasia of the Hip in Models Representing Neonates

Pinak Raodeo
University of Central Florida

ACOUSTIC DETECTION OF DEVELOPMENTAL DYSPLASIA OF THE HIP IN MODELS REPRESENTING NEONATES

by

PINAK PRADIP RAODEO

A thesis submitted in fulfillment of the requirements
for the Honors Interdisciplinary Thesis Program in Mechanical Engineering
in the College of Engineering and Computer Sciences
at the University of Central Florida
Orlando, Florida

Spring Term
2022
Major Professor: Hansen A. Mansy

Abstract

Developmental dysplasia of the hip (DDH) is a condition that involves the dislocation of the head of the femur in the acetabulum of the pelvic bone. Although it may not interfere with a child's range of motion during infancy, DDH can cause various effects over time such as joint pain, abnormal gait, and even paralysis. It is crucial to catch this phenomenon early on so that permanent disability is not introduced to the patient. In this study, an excitation device was used to send a broadband frequency signal through a hip joint simulated by a 3D printed bone apparatus consisting of a left femur and left pelvic bone. Accelerometers were used to sense the transmission of this signal through the bones tested. Variability was induced through different experiments in order to determine where the optimal frequency for detection of DDH would be. After variability was quantified for all of the nonconsecutive and consecutive trials, the excitation device was tested on a raw chicken quarter through the knee joint since this was very similar to the hip joint. Coherence, phase, and transfer function graphs were used to demonstrate the degree of variability, optimal frequencies for detection, and degree of signal transmission through the joints tested. The results from the 3D printed bone model showed that the height of accelerometer suspension, loosened coupling of sensors, and vertical alignment of the bone model apparatus affected the transfer function and phase graphs of the experiments while coherence stayed relatively the same. On the other hand, the results from the raw chicken model displayed similarities between graphs for little to no joint dislocation but the complete dislocation of the bone yielded significantly different graphs.

Acknowledgements

There are many people without whom I could not accomplish this study. I would like to start off by thanking my thesis chair Dr. Hansen Mansy for guiding me through my research journey since my first year at the University of Central Florida. From our weekly meetings to research presentations, he was always someone I could refer to when I needed help on my project. Under his instruction, my experiences as part of the Biomedical Acoustics Research Lab have strengthened my passion for medicine and encouraged me to pursue a medical degree in the future.

I would also like to thank Dr. Charles Price and Dr. Richard Sandler for always being there to consult and advise my team on next steps and recommendations. With their patience and understanding, we have gotten closer to using this technology in a clinical setting and possibly making a difference.

Furthermore, I thank my research team including Tanvir Hassan, Lauren Brown, Maya Hartig, and Matthew Barrow for assisting me through all my experiments and tests during this study. Their cooperation and hard work made this project run smoothly and although there were some obstacles along the way, I am glad we always worked to overcome them.

Finally, I would like to thank all of my friends and family for always being there for me and supporting me through all of my education. Completing this thesis during a pandemic was not an easy task. However, they pushed me to continue chasing my dreams and goals no matter how hard it got, and for that I am utterly grateful.

Table of Contents

LIST OF FIGURES

LIST OF TABLES

CHAPTER 1: INTRODUCTION

The integrity of the hip joint is very important in ensuring physical mobility of any individual. However, any amount of dislocation to the hip can be painful and injurious to the patient, especially if it is not diagnosed immediately. Developmental dysplasia of the hip (DDH) encompasses the defects in hip structure as an individual grows and develops. The most common occurrence associated with this phenomenon is the dislocation of the femur head from the acetabulum of the pelvic bone. There are several different degrees of dislocation due to DDH, and although dislocation of the infant hip can be fairly common. DDH can have several repercussions in adults, such as unbalanced gait, discrepancy in the lengths of the legs, postural issues, and stress on the joints. It is important to screen for DDH as early as possible for it is easier to treat and fix in youth, preferably before the age of six months. This suggestion is based on the fact that the Pavlik Harness cannot be used to repair a dysplastic hip in the case of DDH. In the case that DDH is allowed to progress into adulthood undetected, it will be significantly harder to treat and may even result in permanent disability for the individual. Common treatment for DDH after 18 months of age includes open reduction or hip reconstruction, both of which are invasive procedures lacking a high success rate. (Kotlarsky, Haber, Bialik, & Eidelman, 2015).

Although DDH may seem rare, its incidence in the population is around 36 to 64 per 1000 births according to ultrasonographic detection. Female neonates tend to be at a higher risk for DDH, as are babies that emerge in the breech position and infants who are swaddled tightly, especially in the lower extremities (Yang, Zusman, Lieberman, & Goldstein, 2019). The detection of DDH early on is crucial since this is more benign during infancy, but may become

more severe if not treated early. Failure to provide early treatment may increase the need for surgery of the patient later on, which could result in avascular necrosis in the area, leading to even more instability in the hip joint in these individuals. Even if ultrasound and radiography may help detect DDH, they have been known to take "secondary roles" in terms of diagnosing the abnormality. Generally, doctors will conduct physical examinations which consist of distinction of possible discrepancies in limb length, observation of asymmetrical creases or folds in the thigh or gluteal region, and noting differences in hip abduction or adduction on either side. The Barlow and Ortolani tests also can be used to examine mobility of the joint through a series of movement of the hip, but may not be safe and may not provide significant results (Shaw & Segal, 2016).

The Barlow and Ortolani maneuvers guide physicians in moving around the hip joint of an infant, purposely dislocating the hip and placing it back in the socket using these two respective maneuvers. In the Barlow maneuver, the hip starts out from a fully abducted position and is guided back to a neutral position while the knee is bent but facing the examiner. A slight pressure is placed in the posterior direction with the expectation that if there is hip dysplasia, the hip will be dislocated from the posterior portion of the acetabulum. In the subsequent Ortolani maneuver, the dislocated hip is again abducted from the neutral position but this time anterior and medial pressure is placed on the joint (more specifically the greater trochanters). If the hip was previously dislocated by the Barlow maneuver, the femur head will promptly insert itself into the acetabulum once again. The dislocation and subsequent relocation of a severely dysplastic hip will be signified by clicking sounds as the femoral head is moved out of and back into the acetabulum (Bickley, 2009).

Considering the Barlow and Ortolani maneuvers were created to detect obvious hip dislocation in infants, they may not be able to accurately determine the presence of DDH in more mild cases. Although both maneuvers are designed to detect severe cases of DDH, the diagnosis of a false negative Barlow or Ortolani test may lead to more complications for the patient in the future. Among the 444 infant hip joints tested using the Barlow and Ortolani maneuvers, only 322 were correctly diagnosed. Over 10% of hips tested were proven to be misdiagnosed upon confirmation using ultrasonography (Harper et al., 2020). Although ultrasound can show mild DDH cases in infants, there is a special skillset required to operate this machinery, and technicians who are trained to conduct ultrasound screening may be limited in medically underserved areas. (Kapicioglu & Korkusuz, 2008). For this reason, there must be another cost effective, easy, and efficient method to detect hip dysplasia.

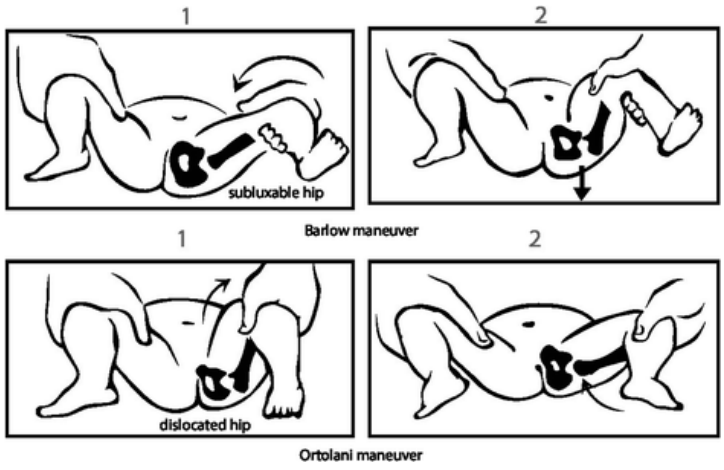

Figure 1. The Barlow and Ortolani maneuvers used to detect DDH are not the most safe or accurate.

A procedure based on the transmission of sound waves through the site of the acetabular joint can be used in lieu of other techniques to detect DDH. Sound can travel through any matter, and the speed at which it travels depends on the density of the medium and the Young's

modulus. The Young's modulus differs significantly between tendon tissue and bone tissue, at 6000 kg/cm^3 and 210000 kg/cm^3 respectively. The acoustic resonance of the tendon tissue will be a lot lower than the acoustic resonance of bone tissue because it will be easier for sound waves to travel through a more porous substance. This means that a dislocated hip can be detected by the absence of bone tissue where it is supposed to be as would be shown by different in sound wave transmission, thus signifying dysplasia (Perez-Oliva, 2016).

Electrosonography can be used to detect dysplasia of the hip in infants. This is accomplished by implementing an electroacoustic generator which transmits broadband white noise with frequencies ranging from 20 to 20,000 Hz up the femur at the location of the patella. There are two signals that detected using accelerometer sensors: one at the symphysis pubis and one at the patella. The infants' hips are positioned at different levels of abduction and adduction in order to optimize the transmission of the signal from the generator. The abduction of the hip from the neutral position aided in sensing the amplitude of the signal. It was observed that the most intense resonance peak across trials was at approximately 410 Hz, and the sound transmission was the highest between the anterior superior iliac spine and the patella. When the knee was flexed at 90 degrees and the hip was abducted at 45 degrees. It was concluded that hips that experienced dysplasia had a larger signal discrepancy as denoted by transfer function as compared to normal, non-dysplastic hips (Kapicioglu & Korkusuz, 2008).

In the study by Hassan from 2018, several exciters, sensors, and models were compared in testing which devices would be most effective in detecting DDH. Of the exciters, it was determined that the one least affected by changes in load, especially in lower frequencies of the

broadband white noise would be the best in exciting the hip joint. Electroacoustic stimulation using the exciter was applied on a 3D printed bone model at the patellar notch while the sensors, located at the patellar notch and iliac crest, respectively, detected the signal as it passed through the bones. The 3D printed model adhered to the resonance and Young's modulus values of anatomical long bones. The experiment involved inducing different levels of hip dysplasia at the acetabular joint, and data was recorded between frequencies of 20 Hz to 2000 Hz using a MATLAB program as displayed below.

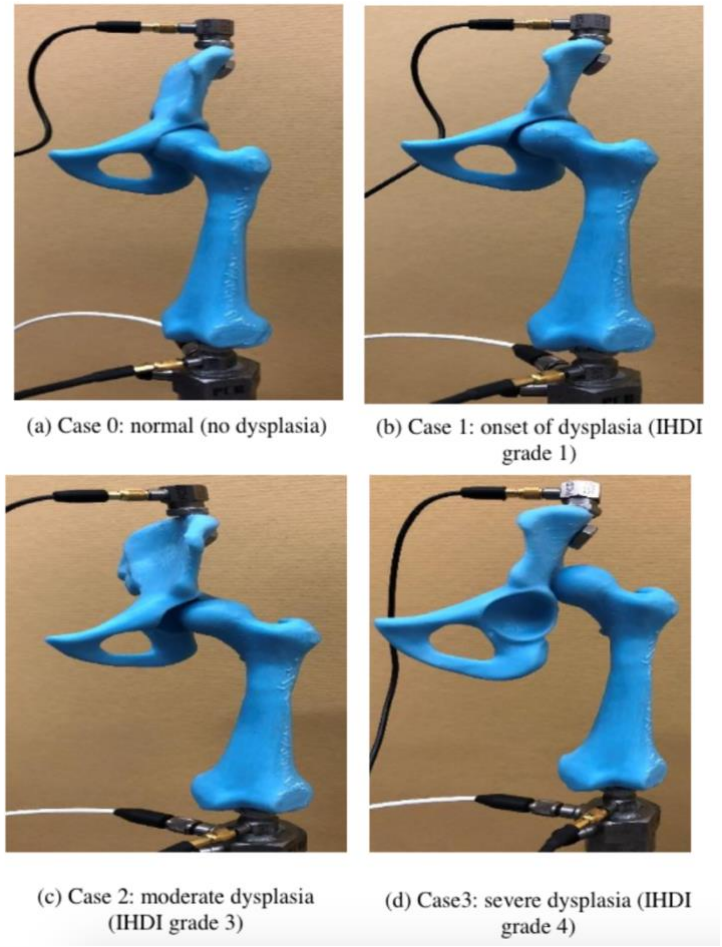

Figure 2. Simulated DDH Cases in a 3D Printed Bone Model (Hassan, 2018).

It was noted that a higher degree of simulated DDH was associated with a less consistent coherence, a leftward shift in the transfer function, and a drop in phase during lower frequencies of the broadband signal as shown in the Figure below:

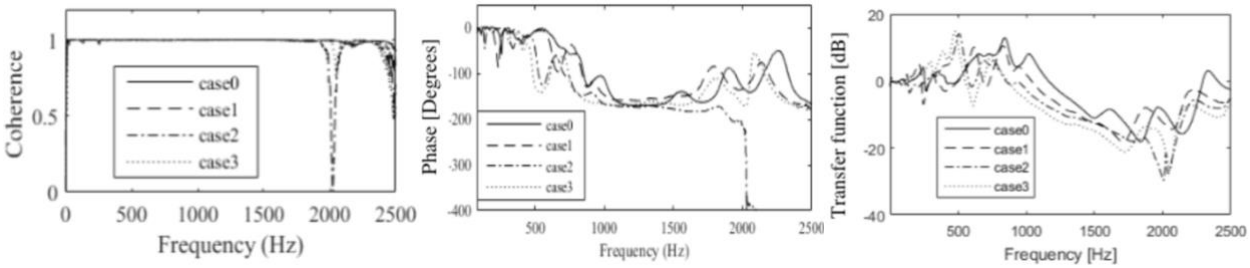

Figure 3. (left to right) Coherence, phase, and transfer function graphs for simulated DDH cases in the 3D printed bone model (Hassan, 2018).

As seen in Figure 3, the last two cases (cases 2 and 3) differ in coherence and transfer function considering the coherence graph has a sharp drop at 2000 Hz for both cases and the transfer function graph has a peak followed by a drop for both cases at around 500 Hz. On the other hand, cases 0 and 1 which demonstrate the least dysplasia are consistently at 1 unit throughout their coherence graphs and their transfer functions have inclines starting at 500 Hz. Also, while the transfer function graph shows cases 2 and 3 reaching their minimums at 2000 Hz, cases 0 and 1 have a hump at this value. Since cases 0 and 1 represent no or mild dysplasia while cases 2 and 3 represent moderate to severe dysplasia, these graphs indicate that this system can be used to differentiate the presence of dysplasia in the 3D hip joint.

Hassan's data was promising in terms of implications of new DDH diagnostics, but did not account for variation due to soft tissue. Studies were later conducted on pig models, but

excitation occurred at the sacrum of the pig where a hole was drilled. This showed significant results in transfer function, coherence, and phase graphs between the left dislocated hip versus the right normal hip. However, the dislocation of the fetal pig hip had to be induced via an invasive procedure in order to test the effectiveness of the device. For instance, the iliofemoral ligament would not be cut or torn in human hip dysplasia cases, but in the pig model, this was the only way to induce severe dislocation, whether through hand pulling or surgery. In addition, there was no synovial fluid in the hip joint of the fetal pig due to preservation, but in a neonatal case, this could play a role in signal transmission through the acetabular joint (Hassan, 2018).

In a study published by Wolters Kluwer Health, whole, raw, free-range chicken models were used to simulate the infant hip due to the ability for the chicken hip to bear weight due to the fully formed and intact synovial capsule in the acetabular joint. This method was introduced in lieu of Baby-Hippy models, which tend to be expensive, and actual neonatal patients who may have been at higher risk considering the coronavirus pandemic. The study involved medical students, residents, and attending physicians using raw chicken joints to test the Barlow and Ortolani maneuvers in substitute for actual neonates. It was concluded by all research participants that the whole raw chicken model was very similar to real infant hip joints, and should be implemented in medical education (Geswell et al., 2020).

Detection of DDH can be accomplished using radiology techniques such as ultrasound and X-rays. However, these methods require special expertise in order to obtain results. In addition, ultrasound tends to be an expensive procedure, deterring low-income families from the detection of DDH early on. X-rays subject the patient to ionizing radiation which is associated

with cancers risks. In addition, both radiography and ultrasound require a special skillset to detect DDH, and may require a hospital visit as opposed to a more convenient visit to the pediatrician. Theoretically, DDH could also be deduced using procedures such as surgery, but invasive procedures require an even higher amount preparation and resources. A method to detect DDH must be created in order to overcome these obstacles, one that is cost-effective, non-invasive, and easy to use.

These experiments will involve inducing variability in a nondysplastic 3D bone case to determine whether these alterations drastically affect the produced data and result in more or less variation between sets of trials than between dysplastic cases. By changing the wire suspension height, loosening the coupling of the sensors used, and tilting the angle of the femur on the 3D bone apparatus, this can be achieved. Following these trials, a soft tissue model of a raw chicken quarter will be used to test variability among nonconsecutive data. Finally, the knee of the chicken quarter will undergo different degrees of dislocation and separation in order to simulate what could occur at an infant joint.

CHAPTER 2: WIRE SUSPENSION OF SENSOR III

2.1 – Objective and Hypothesis

The purpose of this experiment was to examine how the positioning of sensor wires affects the variability in data associated with the transfer function, phase, and coherence graphs generated by the previously created MATLAB DDH detection program. If the wire of sensor III is suspended, then it will exhibit less variability because the items on the table surrounding the apparatus will contribute less to the resonance sensed by the accelerometers. This will result in less interference with signals received from the exciter.

2.2 – Methodology

Sensors II and III were calibrated, placing sensor II on the bottom. The saturation of the signal was constant with no cutoffs and the time domain was consistent, meaning there was a straight horizontal line centered at y=0 with no settling. When the calibration resulted in a coherence graph with a value of 1 unit throughout and a transfer function of around zero, experimentation was started. Sensor II was placed face down onto the iLouder exciter using minimal accelerometer wax, and 0.1 g of wax was used to attach the back of sensor II to the patellar notch of the 3D printed left femur. The head of the femur was attached to the center of the acetabulum using 0.2 g of accelerometer wax and a flair pen was used to outline the crest of the acetabulum onto the left femur head for consistency of placement later on. The 20 cm point on the wire attached to the head of sensor III was marked using tape. A ring stand was marked 30 cm, 20 cm, 10 cm, and 0 cm above the base of the exciter using a permanent marker. The tape on

the wire was aligned with the 30 cm mark of the ring stand and attached using tape. Sensor III's face was then attached to the nut on top of the iliac crest using 0.1 g of accelerometer wax, but the wire was not taut. The MATLAB DDH detection program was used to run 3 back-to-back trials for each suspension height, and the apparatus was not altered at all during these. Three back-to-back trials made up one set of trials, which were nonconsecutive with other sets. Between two nonconsecutive sets, sensors II and III were removed from the bone apparatus and the femur was taken out of the acetabulum. The apparatus was reassembled at the beginning of each nonconsecutive set of 3 back-to-back trials, and pictures were taken to ensure consistency of setups. The MATLAB DDH compare function was used to compare the coherence, phase, and transfer functions of the three trials in each set, and then the first run of each nonconsecutive set. The comparison of the coherence, phase, and transfer function graphs for each height of suspension of the sensor III wire was also observed for the first run of each nonconsecutive set.

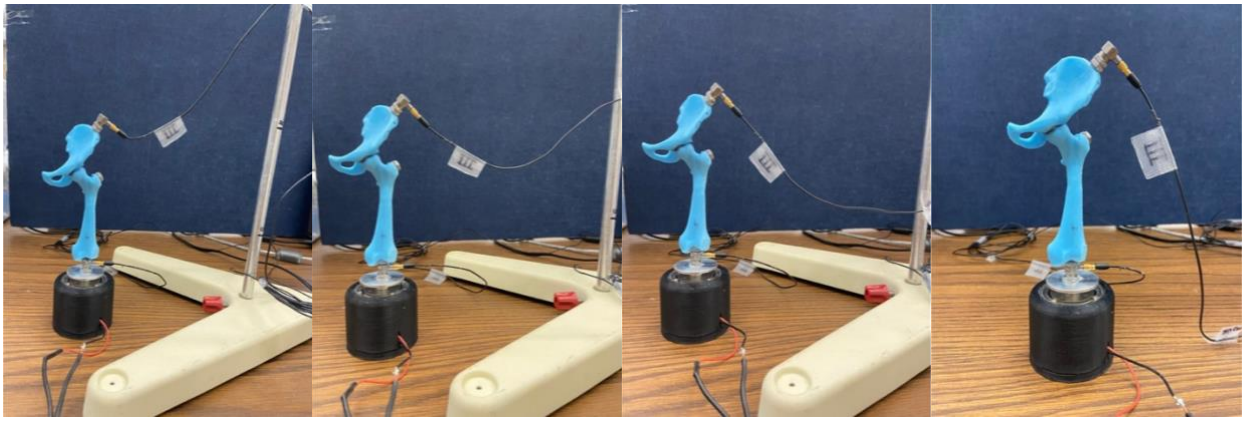

Figure 4. Experimental setup for altered sensor III wire suspension heights of 30 cm, 20 cm, 10 cm and 00 cm respectively.

2.3 – Data

Suspension at 30 cm: Sets 0, 1, and 2

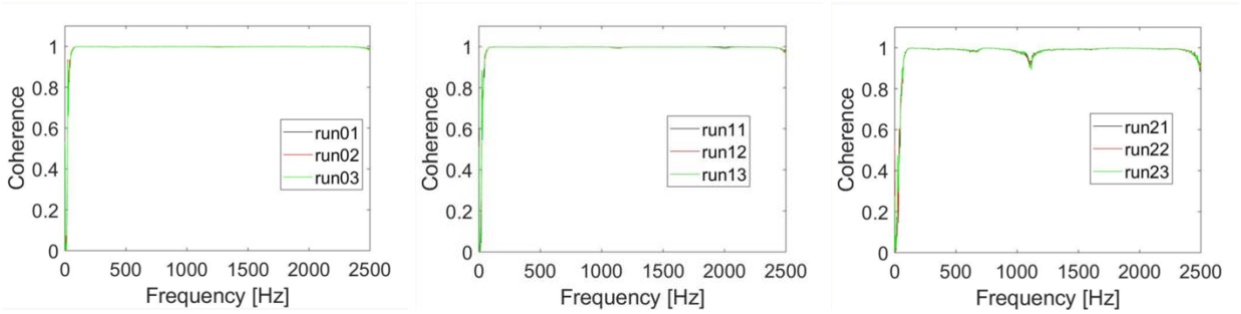

Figure 5. Coherence graphs for back-to-back trials for 30 cm wire suspension.

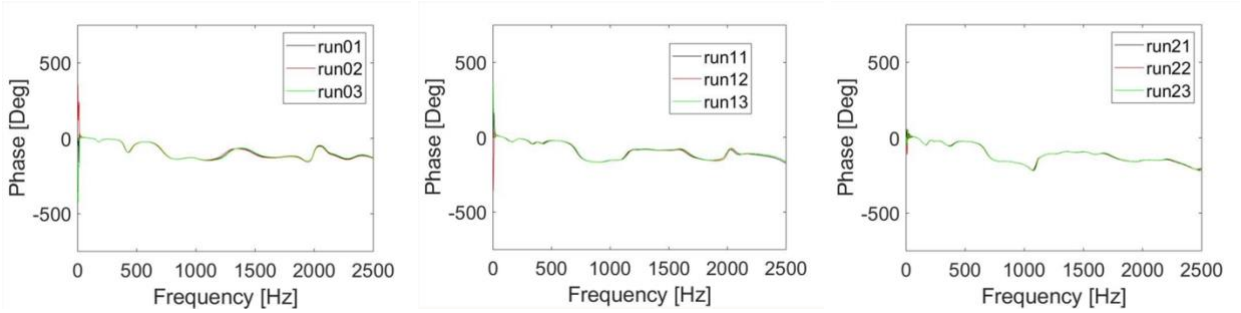

Figure 6. Phase graphs for back-to-back trials for 30 cm wire suspension.

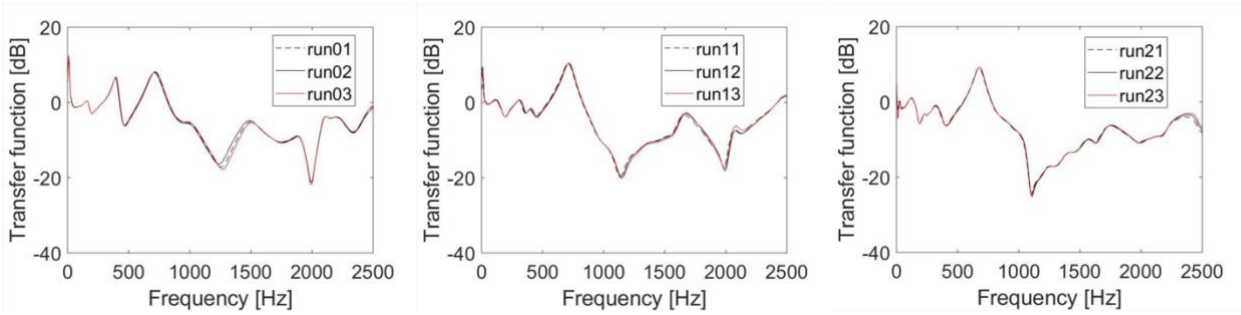

Figure 7. Transfer function graphs for back-to-back trials for 30 cm wire suspension.

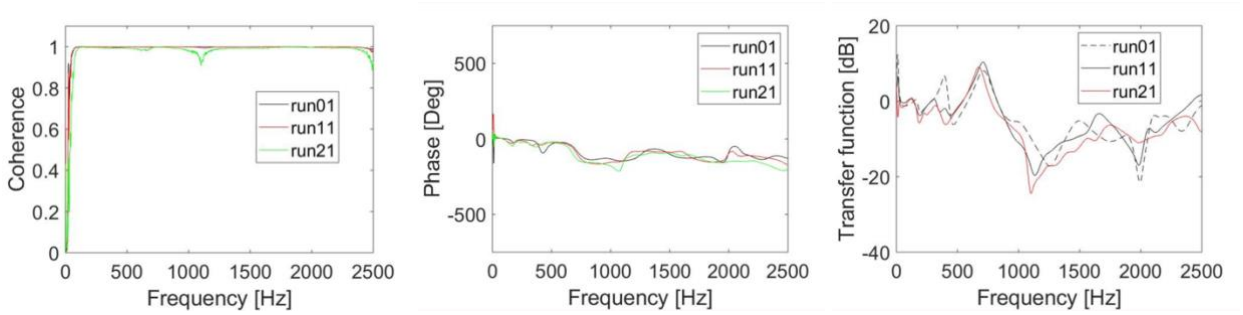

Figure 8. (left to right) Coherence, phase, and transfer function graphs for the first run of each nonconsecutive set for 30 cm wire suspension.

Suspension at 20 cm: Sets 0, 1, and 2

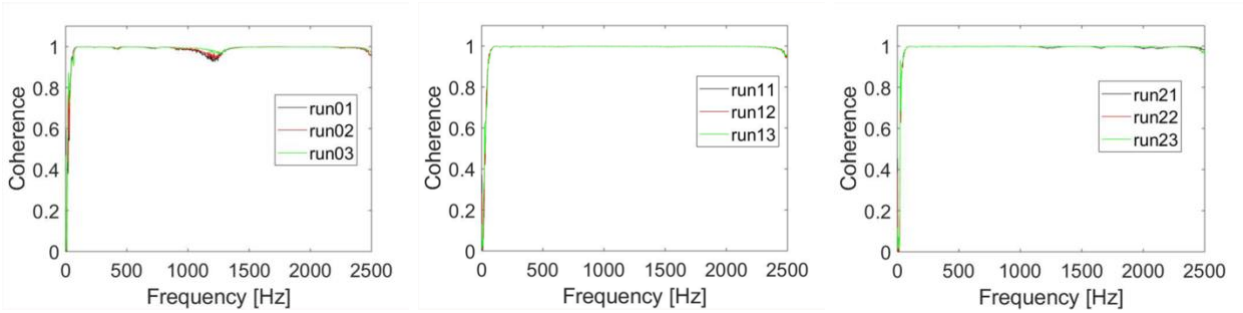

Figure 9. Coherence graphs for back-to-back trials for 20 cm wire suspension.

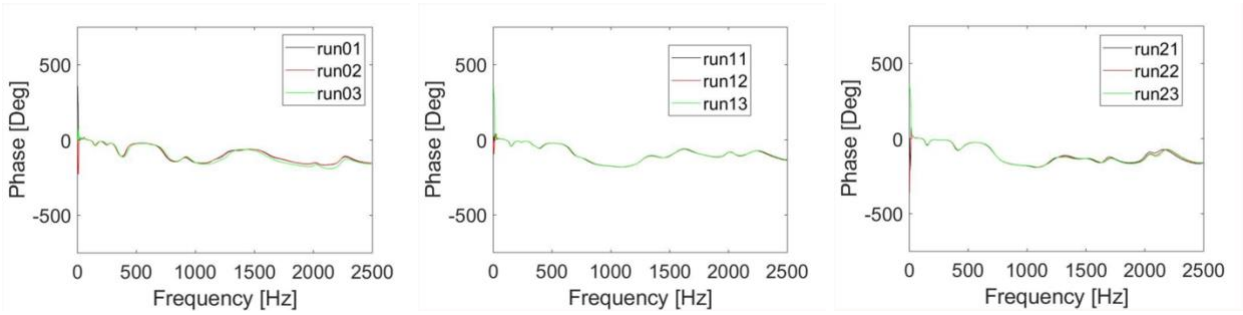

Figure 10. Phase graphs for back-to-back trials for 20 cm wire suspension.

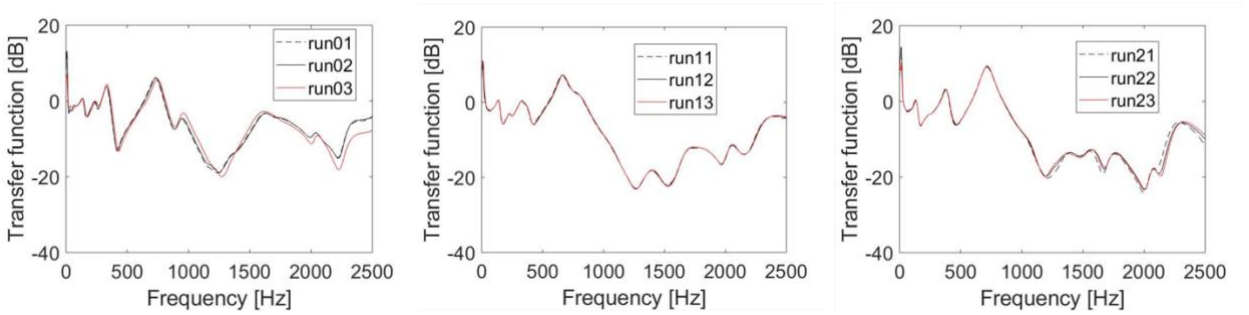

Figure 11. Transfer function graphs for back-to-back trials for 20 cm wire suspension.

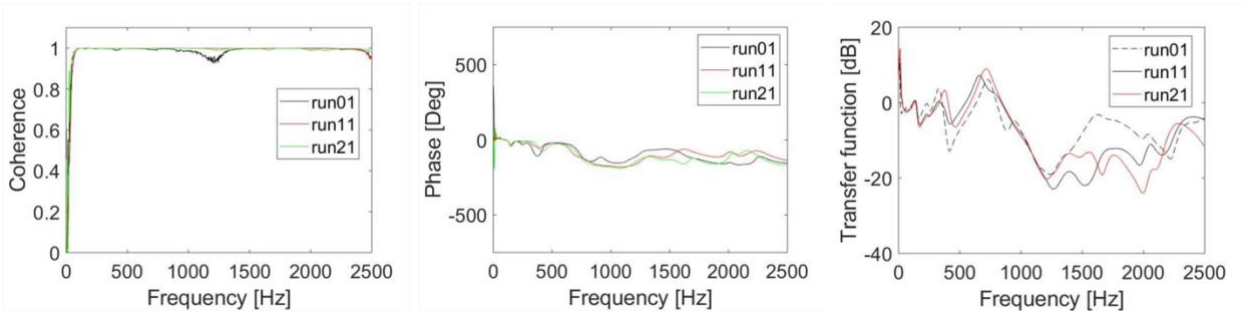

Figure 12. (left to right) Coherence, phase, and transfer function graphs for the first run of each nonconsecutive set for 20 cm wire suspension.

Suspension at 10 cm: Sets 0, 1, and 2

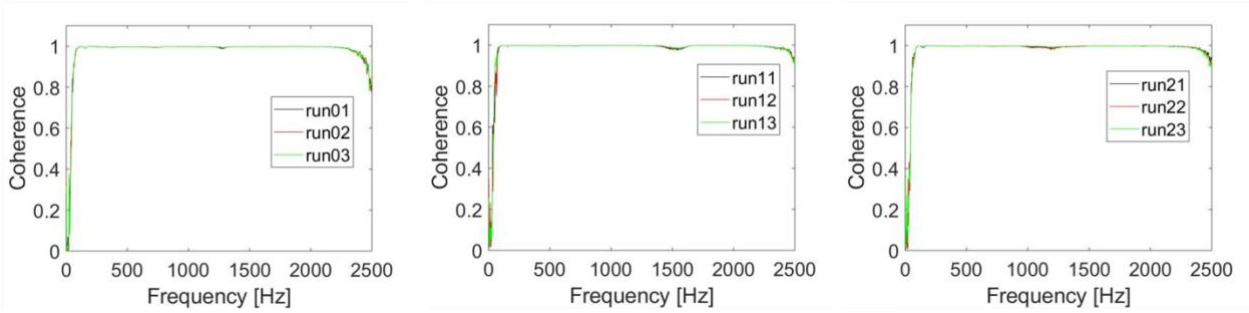

Figure 13. Coherence graphs for back-to-back trials for 10 cm wire suspension.

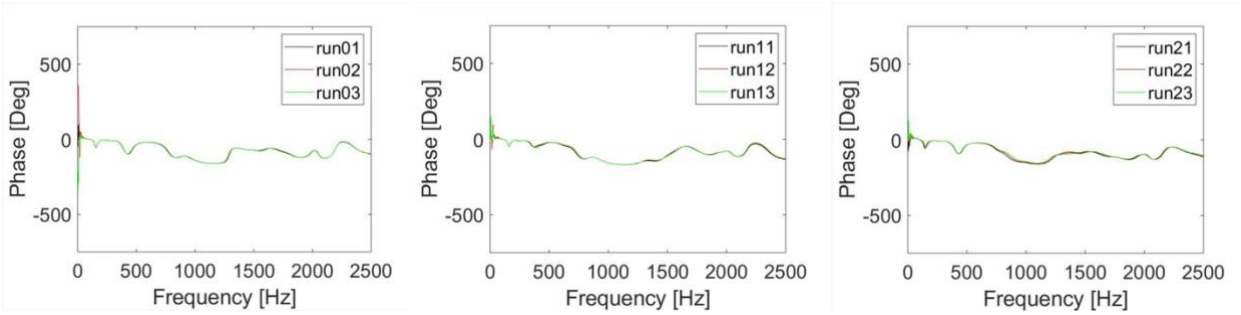

Figure 14. Phase graphs for back-to-back trials for 10 cm wire suspension.

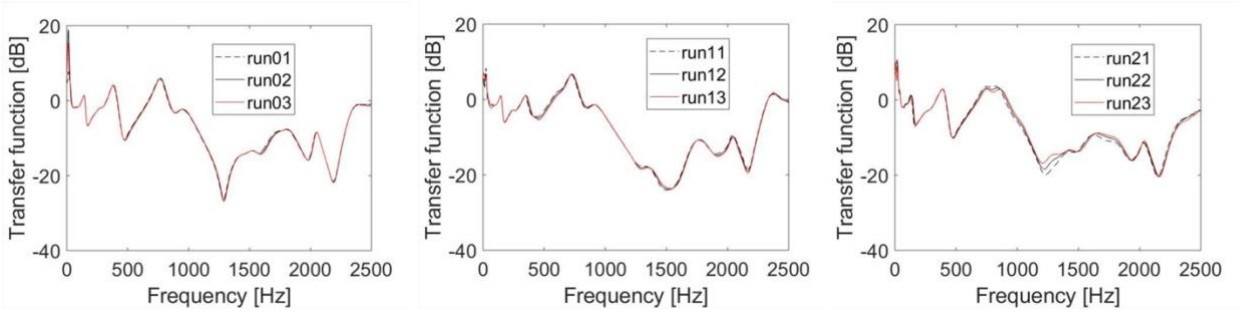

Figure 15. Transfer function graphs for back-to-back trials for 10 cm wire suspension.

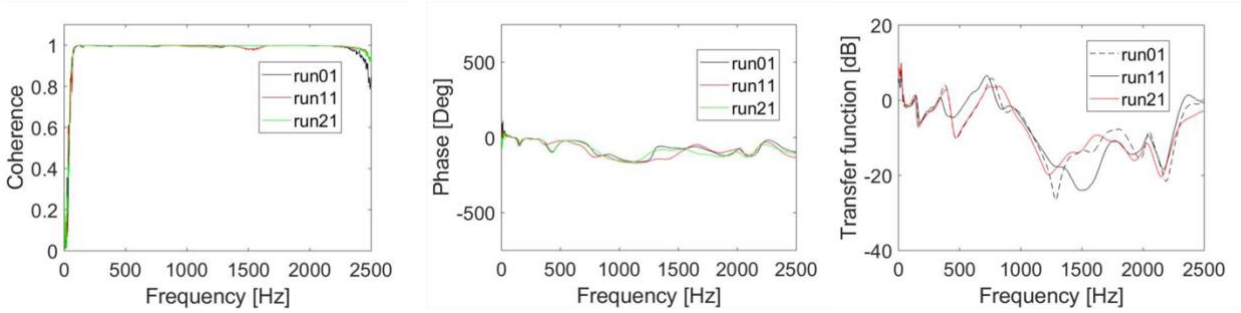

Figure 16. (left to right) Coherence, phase, and transfer function graphs for the first run of each nonconsecutive set for 10 cm wire suspension.

Suspension at 0 cm: Sets 0, 1, and 2

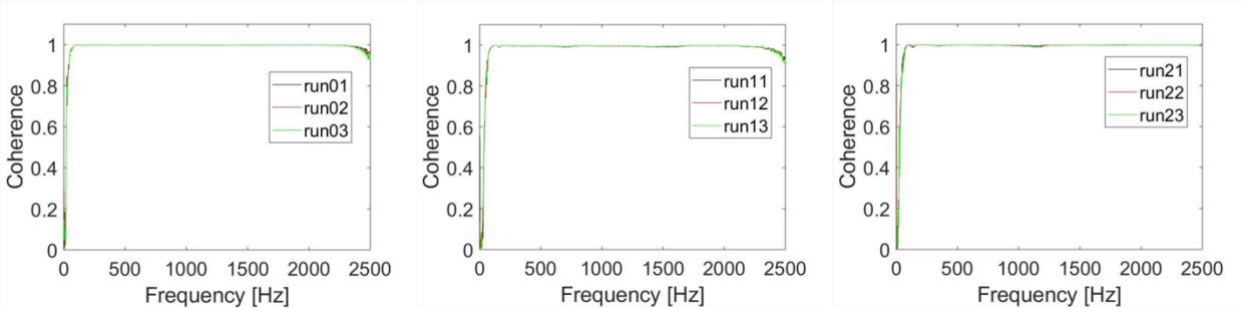

Figure 17. Coherence graphs for back-to-back trials for 0 cm wire suspension.

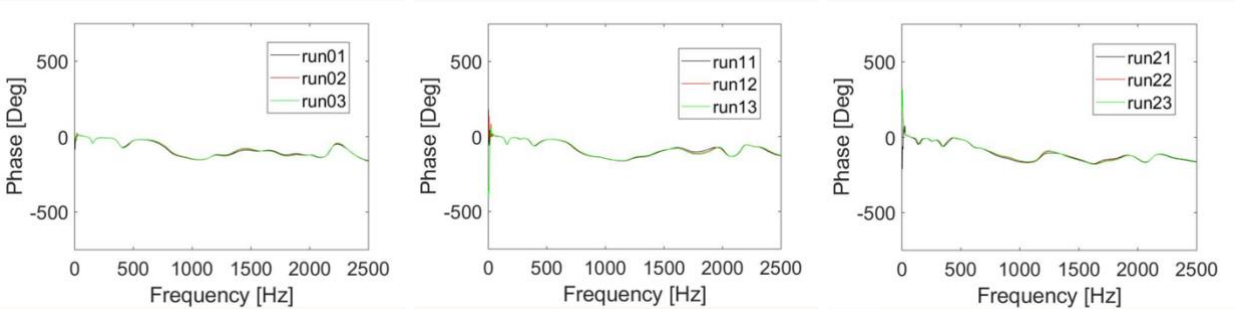

Figure 18. Phase graphs for back-to-back trials for 0 cm wire suspension.

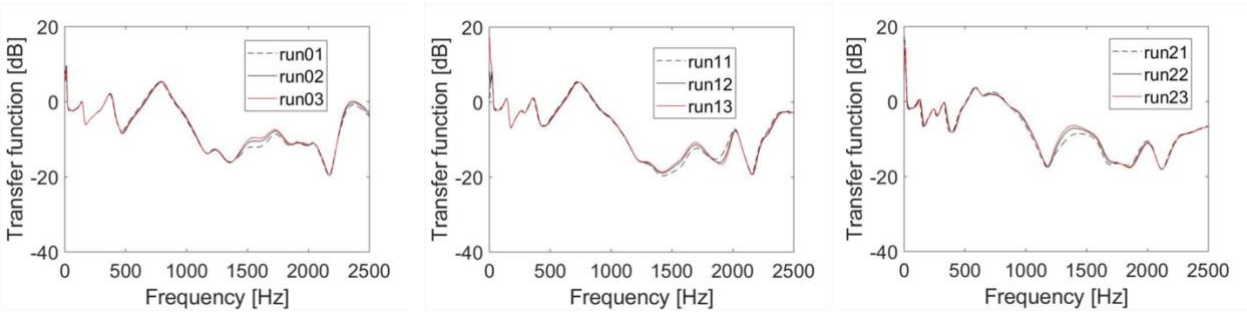

Figure 19. Transfer function graphs for back-to-back trials for 0 cm wire suspension.

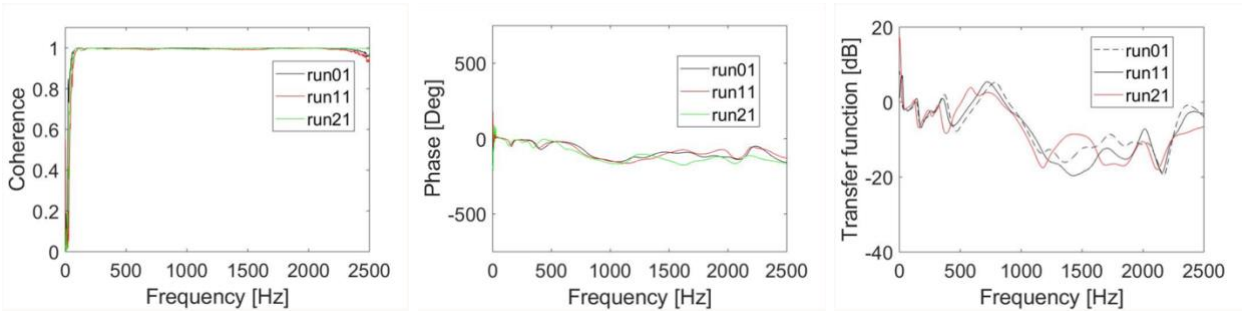

Figure 20. (left to right) Coherence, phase, and transfer function graphs for the first run of each nonconsecutive set for 0 cm wire suspension.

Comparison across All Suspension Heights

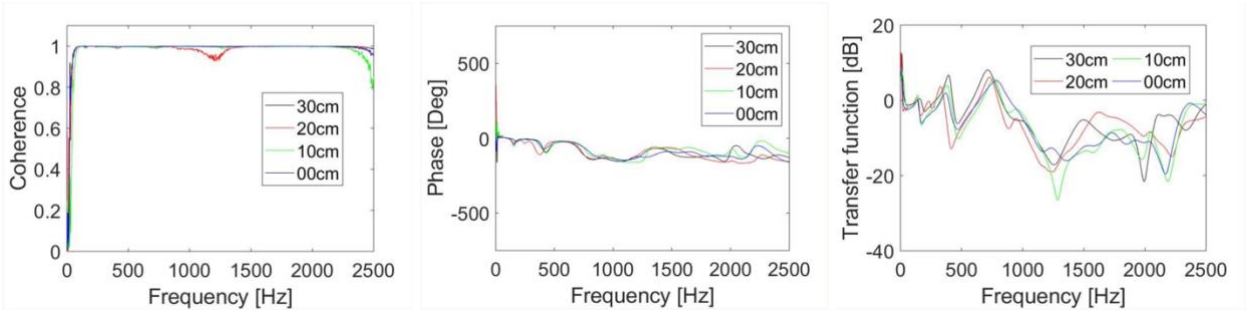

Figure 21. (left to right) Coherence, phase, and transfer function graphs for run 01 of each different sensor III wire suspension height, including 30 cm, 20 cm, 10 cm, and 0 cm suspension.

Table 1. Quantified Variability of Transfer Functions between Nonconsecutive Sets for Different Wire Suspensions

Runs Compared	Average Value of Differences between 50-500 Hz [dB]	Average Value of Differences between 501-1100 Hz [dB]	Average Value of Differences between 1101 – 2000 Hz [dB]
30 cm - 01, 11, 21	1.6247	1.053533333	1.2463
20 cm – 01, 11, 21	0.519666667	1.531733333	4.9871
10 cm – 01, 11, 21	0.262133333	0.9708	1.7386
00 cm – 01, 11, 21	0.4016	0.3726	1.9133

2.4 – Analysis and Discussion

All of the back to back trials performed across different wire suspensions were relatively consistent; however, when the first runs of each of the nonconsecutive sets were compared to each other, they were not as similar. It was seen that the variability between the first runs of each nonconsecutive set was notably lower at a reduced height of wire suspension as seen in Table 1. For instance, at 00 cm and 10 cm there is only an average difference of 0.401 and 0.262, respectively. An exception to this rule was the data that was obtained at the higher frequencies (1100-2000 Hz) which was more variable overall and displayed an opposite trend to what was seen before. This may have been due to the fact that at sound waves of higher frequencies, there is a greater signal to noise ratio that causes additional interference. Also, greater frequencies of sound have more energy than lower frequencies, so this could contribute to the variation as well. Although the first runs of each nonconsecutive set for the 501-1100 Hz had lower average difference at the 30 cm wire suspension height, Table 1 still demonstrated that in the 50-500 Hz range, the variability decreased with wire suspension height. However, the average differences between the 501-1100 Hz range were still higher than those of the 50-500 Hz range (Table 1). Because the variability of the nonconsecutive sets between 50-500 Hz frequency range seems like it was the least overall, this may be the optimal range of frequency to use in order to detect DDH in the infant hip since it was the most consistent overall when testing the intact 3D printed bone apparatus joint.

CHAPTER 3: LOOSENED SENSOR II COUPLING

3.1 – Objective and Hypothesis

The purpose of this experiment was to observe how loosening of the nut on sensor II affected the variability of coherence, phase, and transfer function data generated by the MATLAB DDH detection program. If sensor II was loosened, the degree of loosening of its nut will correspond to the extent of variation in the data because the excitation signal from the iLouder will not be accurately detected by the loosened accelerometer.

3.2 – Methodology

Sensors II and III were calibrated one on top of the other, and the saturation was ensured to be constant with no cutoffs. The time domain was also consistent with no settling, and when the calibration yielded a coherence of 1 unit and a transfer function of zero dB throughout the corresponding graphs, the experiment was commenced. Using a permanent fine tip marker, a mark was made perpendicularly intersecting the side of sensor II where the nut attaches to the rest of the sensor. Two marks were made 15 degrees and 30 degrees past this initial mark using the marker and a protractor. Sensor II was placed face down onto the iLouder exciter using minimal accelerometer wax, and the back of sensor II was attached to the patellar notch of the 3D printed left femur using 0.1 g of wax. 0.2 g of accelerometer wax was used to attach the center of the left femoral head to the center of the acetabulum and the crest of the acetabulum was traced along the head of the femur in order to maintain consistency between sets. Sensor III was attached to the nut on top of the iliac crest using another 0.1 g of wax, but the wire was not kept taut. The MATLAB DDH program was conducted for one run before turning sensor II 15

degrees and running it again. After loosening for one run, the sensor II nut was tightened back to the original position for another run; sensor II was loosened to 15 degrees one more time to complete the trials for the set. Between each set, the apparatus of 3D printed bones and sensors was disassembled and then reassembled. If the sensors came off or if the bone apparatus tilted or fell off in any way, the set was repeated. A total of three nonconsecutive sets of data were obtained for this, and the procedure was repeated for 30 degrees as well.

Figure 22. General experimental setup for loosened sensor II coupling.

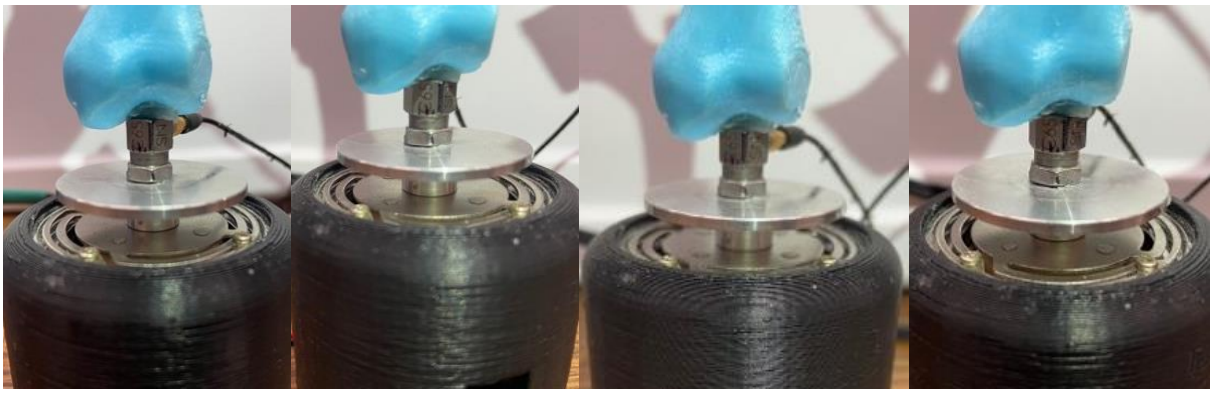

Figure 23. Demonstrated loosened sensor II coupling by 15 degrees within a single set (0 > 15 > 0 > 15)

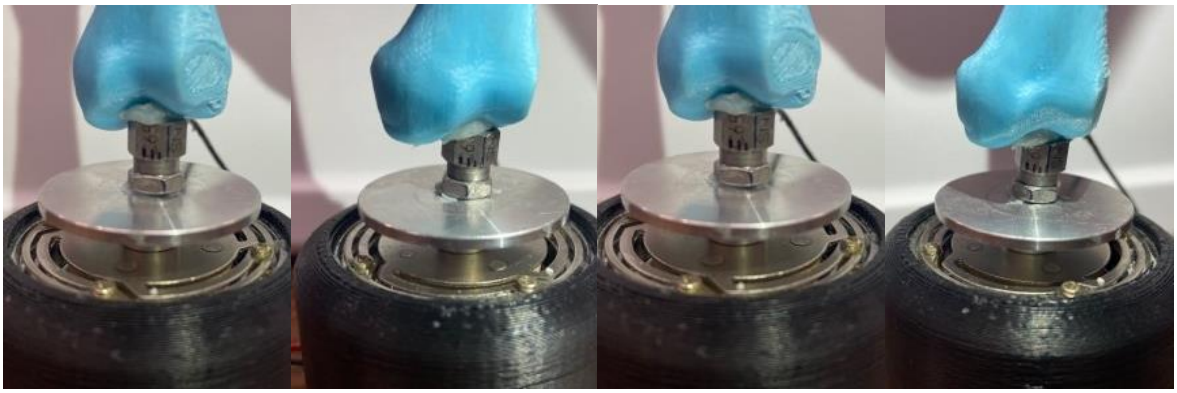

Figure 24. Demonstrated loosened sensor II coupling by 30 degrees within a single set (0 > 30 > 0 > 30)

3.3 – Data

Loosened Sensor II Coupling by 15 Degrees

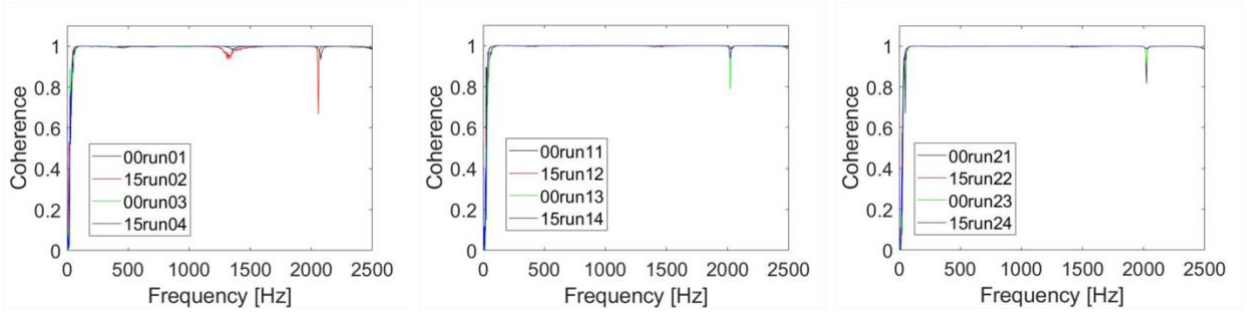

Figure 25. Coherence graphs for loosened sensor II coupling from 0 to 15 degrees within sets 0, 1, and 2.

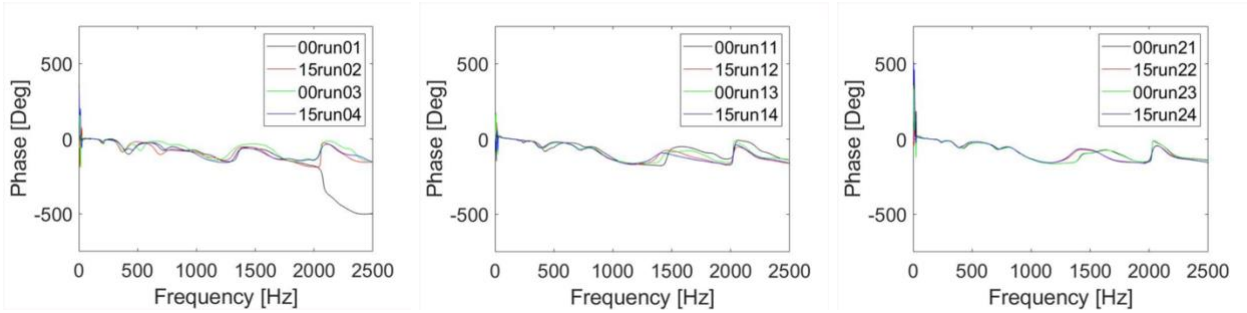

Figure 26. Phase graphs for loosened sensor II coupling from 0 to 15 degrees within sets 0, 1, and 2.

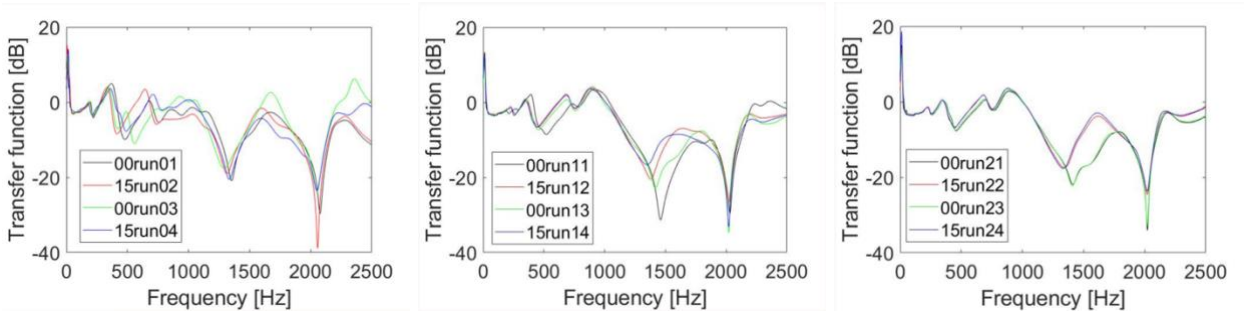

Figure 27. Transfer function graphs for loosened sensor II coupling from 0 to 15 degrees within sets 0, 1, and 2.

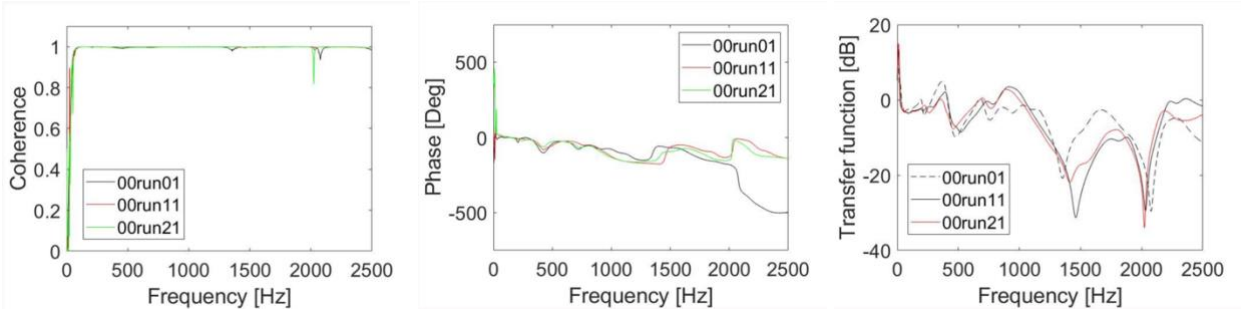

Figure 28. Coherence, phase, and transfer function graphs for run 1 of each nonconsecutive set for when sensor II was at its original position (0 degrees) before loosening it by 15 degrees.

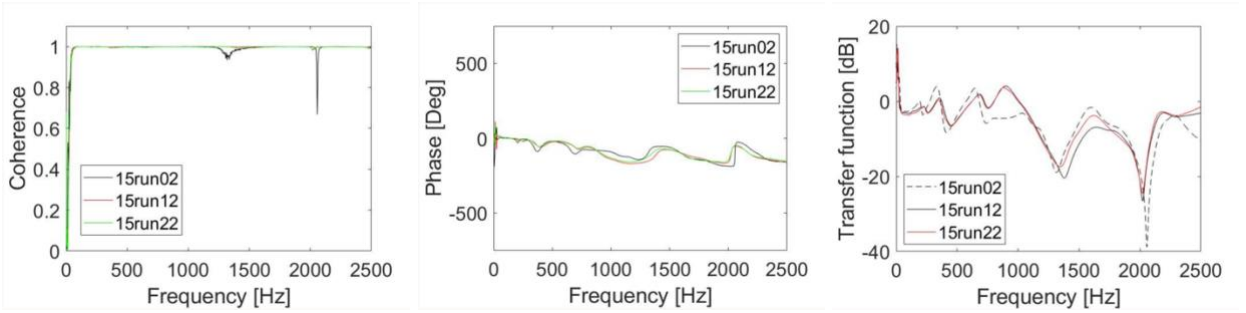

Figure 29. (left to right) Coherence, phase, and transfer function graphs for run 2 of each nonconsecutive set for when sensor II was loosened by 15 degrees for the first time.

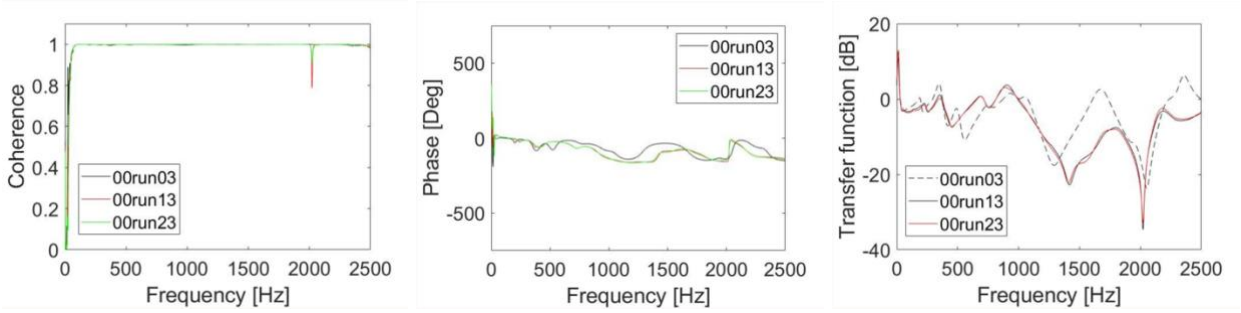

Figure 30. (left to right) Coherence, phase, and transfer function graphs for run 3 of each nonconsecutive set for when sensor II was twisted back to its original position (0 degrees) after being loosened by 15 degrees.

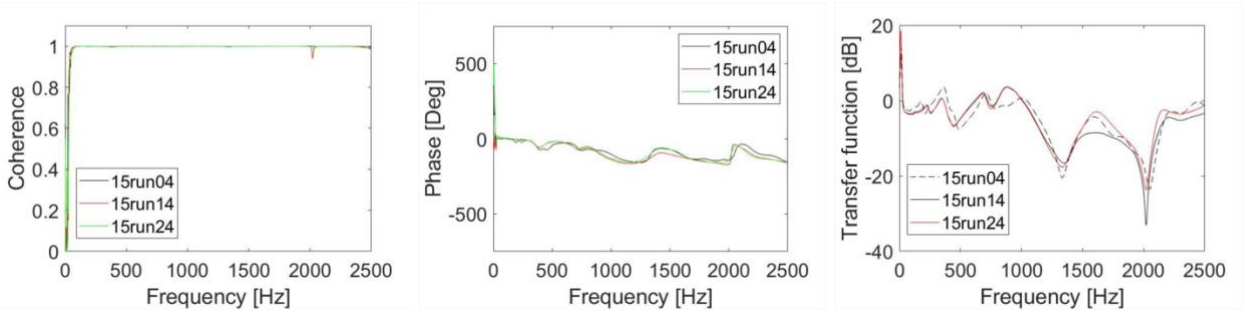

Figure 31. (left to right) Coherence, phase, and transfer function graphs for run 4 of each nonconsecutive set for when sensor II was loosened by 15 degrees for the last time.

Loosened Sensor II Coupling by 30 Degrees

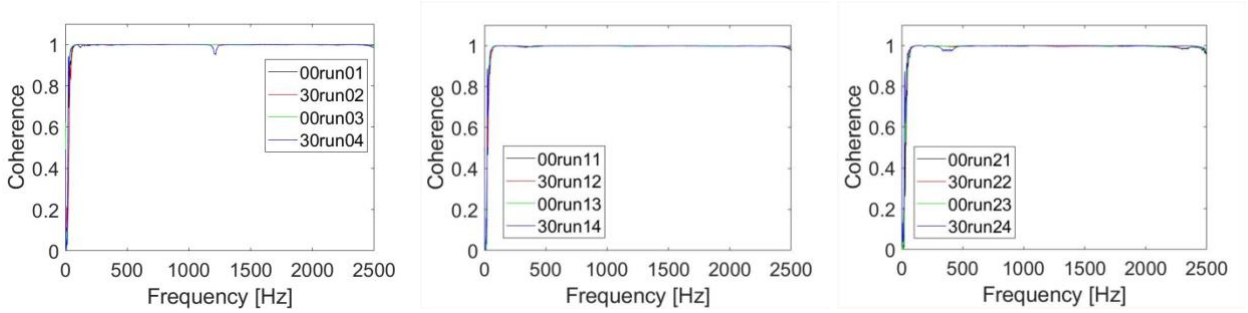

Figure 32. Coherence graphs for loosened sensor II coupling from 0 to 30 degrees within sets 0, 1, and 2.

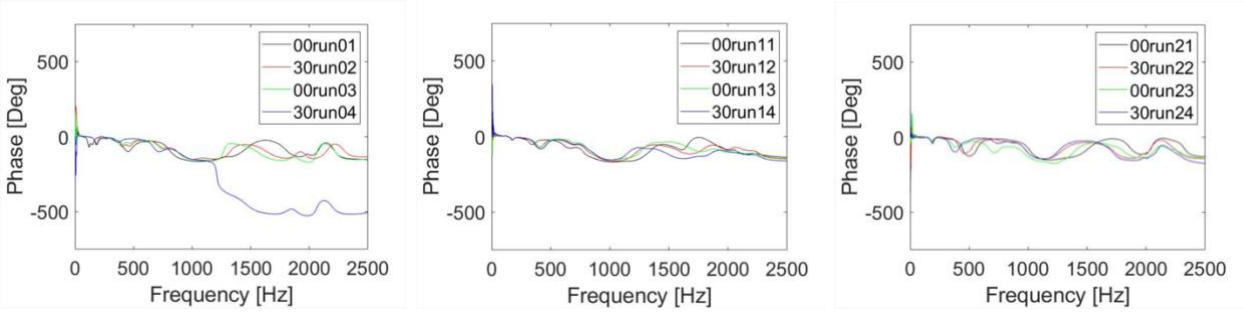

Figure 33. Phase graphs for loosened sensor II coupling from 0 to 15 degrees within sets 0, 1, and 2.

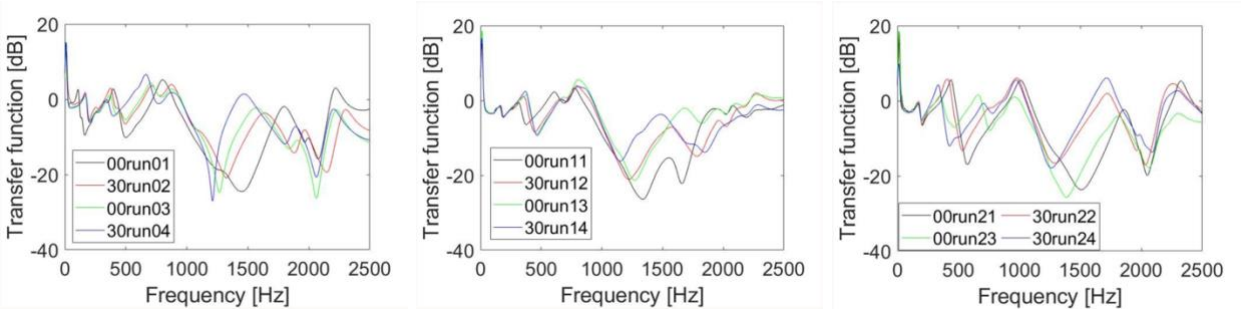

Figure 34. Transfer function graphs for loosened sensor II coupling from 0 to 30 degrees within sets 0, 1, and 2.

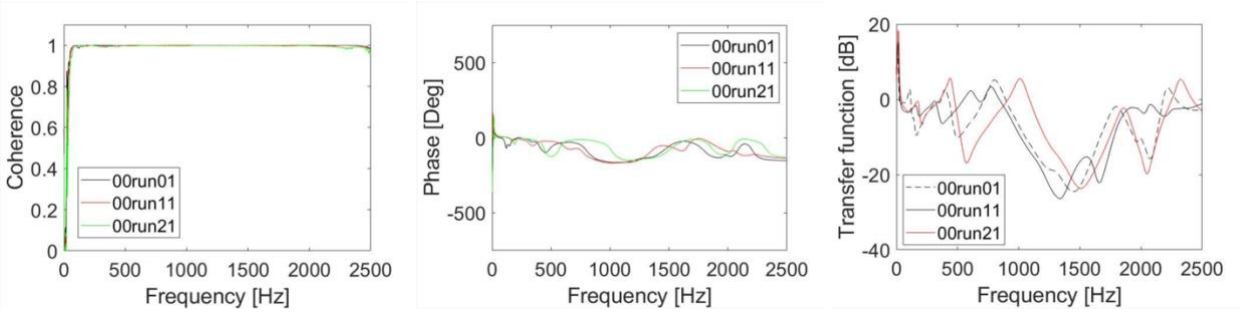

Figure 35. (left to right) Coherence, phase, and transfer function graphs for run 1 of each nonconsecutive set for when sensor II was at its original position (0 degrees) before loosening it by 30 degrees.

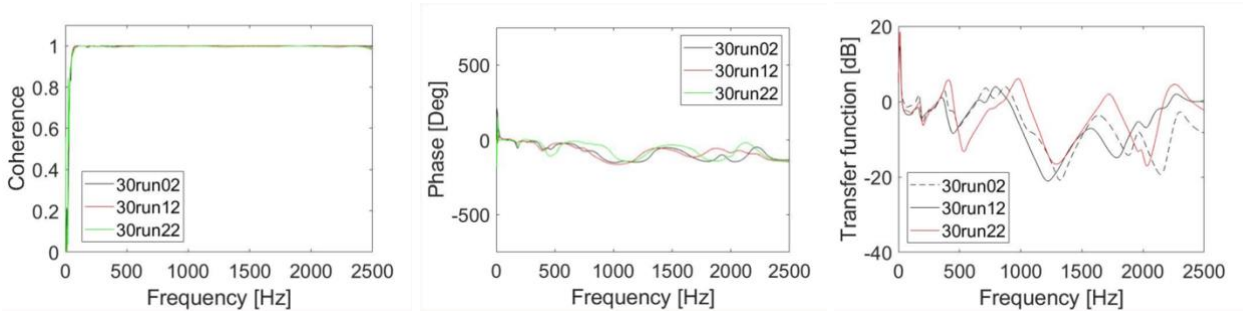

Figure 36. (left to right) Coherence, phase, and transfer function graphs for run 2 of each nonconsecutive set for when sensor II was loosened by 30 degrees for the first time.

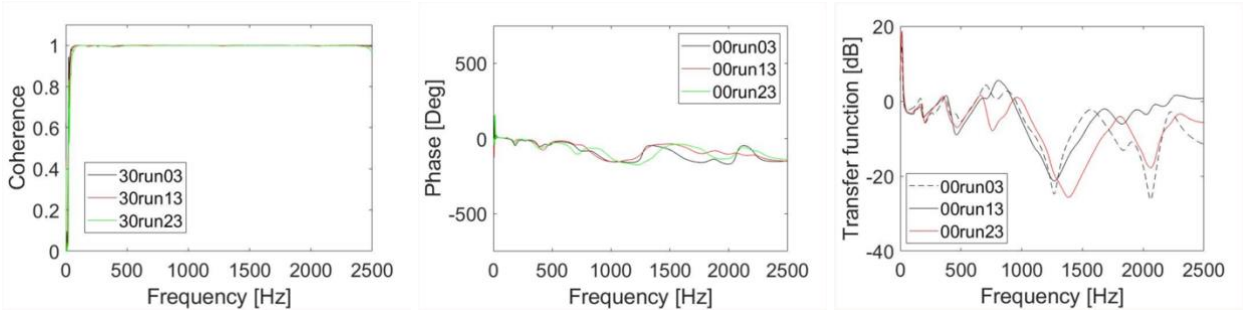

Figure 37. (left to right) Coherence, phase, and transfer function graphs for run 3 of each nonconsecutive set for when sensor II was twisted back to its original position (0 degrees) after being loosened by 30 degrees.

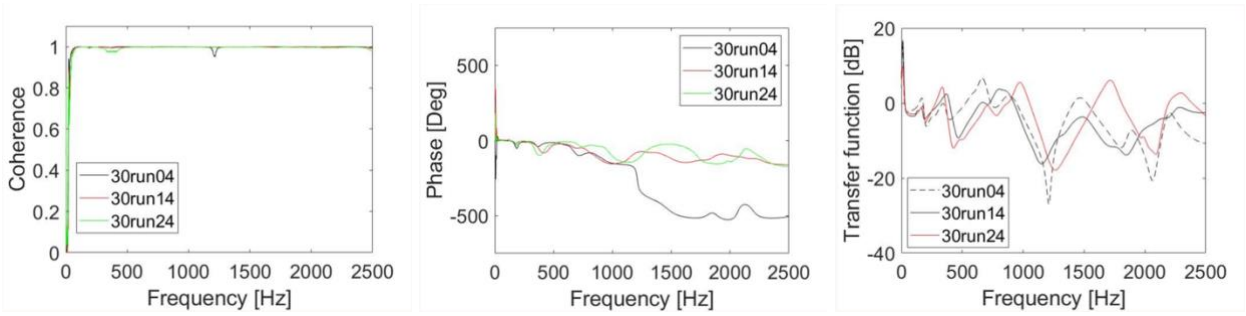

Figure 38. (left to right) Coherence, phase, and transfer function graphs for run 4 of each nonconsecutive set for when sensor II was loosened by 30 degrees for the last time.

Table 2. Quantified Variability of Transfer Functions between Nonconsecutive Sets for Loosened Sensor II Coupling of 15 Degrees

Runs Compared	Average Value of Differences between 50-500 Hz [dB]	Average Value of Differences between 501-1100 Hz [dB]	Average Value of Differences between 1101 – 2000 Hz [dB]
00 degrees - 01, 11, 21	0.9882	1.427133333	4.1301
15 degrees - 02, 12, 22	0.510066667	1.9834	1.7162
00 degrees – 03, 13, 23	0.8966	1.341933333	3.739
15 degrees – 04, 14, 24	1.0776	1.037133333	1.0999

Table 3. Quantified Variability of Transfer Functions between Nonconsecutive Sets for Loosened Sensor II Coupling of 30 Degrees

Runs Compared	Average Value of Differences between 50-500 Hz [dB]	Average Value of Differences between 501-1100 Hz [dB]	Average Value of Differences between 1101 – 2000 Hz [dB]
00 degrees - 01, 11, 21	1.410733333	1.5444	1.7519
30 degrees - 02, 12, 22	1.387266667	0.9884	3.0505
00 degrees – 03, 13, 23	0.346866667	1.2762	2.8604
30 degrees – 04, 14, 24	0.805266667	1.430533333	2.472

3.4 – Analysis and Discussion

In this experiment, the loosening of the nut on sensor II to alter coupling resulted in production of variation in the transfer function and phase graphs. Although coherence stayed relatively the same across both the back-to-back and nonconsecutive trials, there was variation in both the phase and transfer functions across all back-to-back and nonconsecutive trials. This was largely due to the interference of signal detection exacerbated by the loosening of the nut, which caused the variation in the graphs. Across the different groups of runs in nonconsecutive sets, there does not seem to be a trend as to which run numbers produced the most variation in the transfer functions when it came to a loosened coupling of 15 degrees or 30 degrees. The variation when comparing the same range of frequencies for 15 degrees of loosened coupling

versus 30 degrees of loosened coupling did not differ significantly as observed in Table 2 and Table 3. However, it was observed that there was an increased average difference between nonconsecutive runs as the ranges of frequencies increased. In other words, there was lower variability between nonconsecutive runs in the 50-500 Hz range and the most variability in the 1100-2000 Hz range. This may have been due to the higher sound frequencies having a higher signal to noise ratio that caused higher levels of variations in this region. Lower frequencies have a lower signal to noise ratio that results in less variability between the transfer function of nonconsecutive trials. This further illustrates that the 50-500 Hz range is optimal for the detection of DDH because even though the coupling of sensor II was loosened relatively dramatically, it often resulted in an average difference of 1 dB or less in the transfer function graphs among the different nonconsecutive runs.

CHAPTER 4: LOOSENED SENSOR III COUPLING

4.1 – Objective and Hypothesis

The point of this experiment was to determine if the loosening of sensor III on the 3D printed bone apparatus has an effect on the variability of the coherence, phase, and transfer function data obtained from the MATLAB program for DDH detection. If sensor III was loosened, the extent of how much it is loosened will correlate to the amount of variation in data because sensor III will not be able to accurately detect the iLouder's excitation signal.

4.2 – Methodology

Sensors II and III were placed on top of the other and calibrated while it was made sure that the saturation of the signal was constant with no cutoffs. The time domain was ensured to be constant with no settling. When the calibration graphs were observed to have a coherence of 1 unit and a transfer function of zero dB, the experiment was allowed to proceed. A permanent fine tip marker was used to perpendicularly intersect the side of sensor III where the nut was attached to the rest of the accelerometer. Marks were made 15 degrees and then 30 degrees past this initial mark with the help of a protractor and the same marker. Sensor II was attached face down onto the iLouder using the minimal amount of accelerometer wax, and its back was attached to the patellar notch of the left femur using 0.1 g of wax. Another 0.2 g of wax stabilized the center of the left femoral head in the center of the left acetabulum. The acetabular crest was traced along the head of the femur so that setups would be consistent throughout the experiment. Sensor III started off tightened with its perpendicularly intersecting line intact, and placed on top of the iliac crest using 0.1 g of accelerometer wax. The MATLAB DDH detection program was run for

one trial before loosening sensor III by rotating it 15 degrees and conducting another run. After this run, sensor III was tightened back to the original 0 degree mark, ran once again, and loosened to 15 degrees one last time to complete the first set of trials. Between sets, the apparatus was completely taken apart and put back together. If the apparatus fell apart or fell down in any way, the entire set of data had to be obtained again. A total of three nonconsecutive sets of data were produced, and this entire protocol was repeated but instead of loosening sensor III by 15 degrees, it was loosened by 30 degrees.

Figure 39. All of the experimental setups demonstrated looked like the picture shown. The only alteration was the rotation of sensor III on the top to loosen coupling of the accelerometer.

Figure 40. Demonstrated loosened sensor III coupling by 15 degrees within a single set (0 > 15 > 0 > 15)

Figure 41. Demonstrated loosened sensor III coupling by 30 degrees within a single set (0 > 30 > 0 > 30)

4.3 – Data

Loosened Sensor III Coupling by 15 Degrees

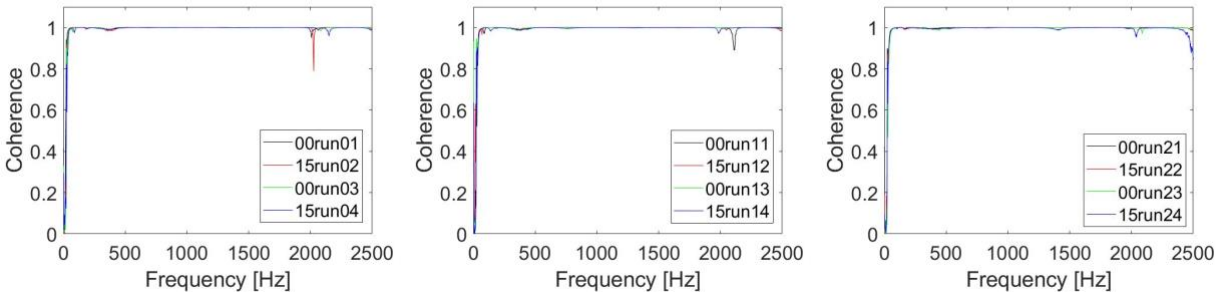

Figure 42. Coherence graphs for loosened sensor III coupling from 0 to 15 degrees within sets 0, 1, and 2.

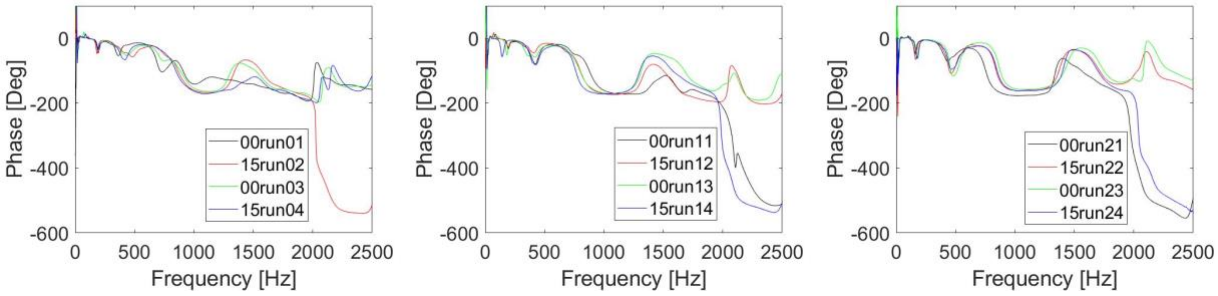

Figure 43. Phase graphs for loosened sensor III coupling from 0 to 15 degrees within sets 0, 1, and 2.

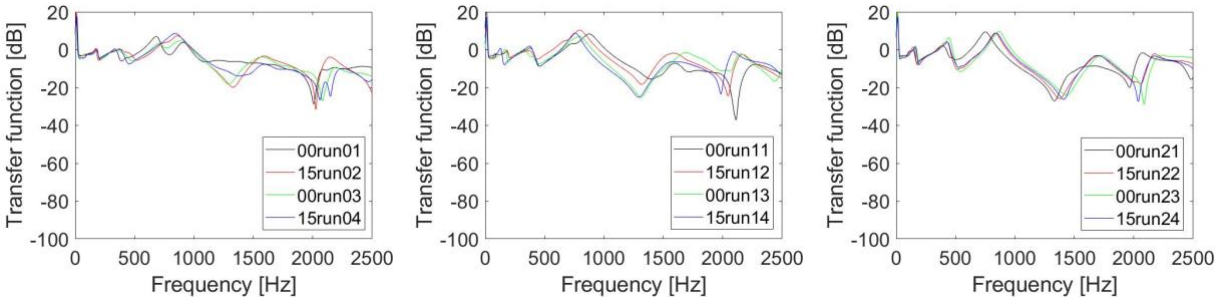

Figure 44. Transfer function graphs for loosened sensor III coupling from 0 to 15 degrees within sets 0, 1, and 2.

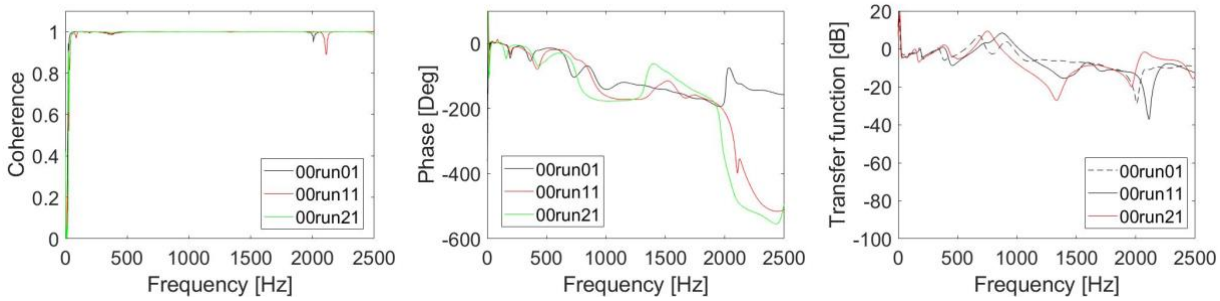

Figure 45. (left to right) Coherence, phase, and transfer function graphs for run 1 of each nonconsecutive set for when sensor III was at its original position (0 degrees) before loosening it by 15 degrees.

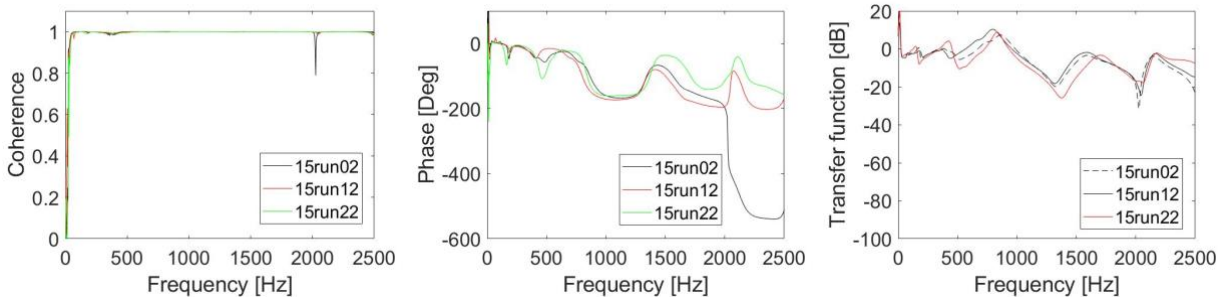

Figure 46. (left to right) Coherence, phase, and transfer function graphs for run 2 of each nonconsecutive set for when sensor III was loosened by 15 degrees for the first time.

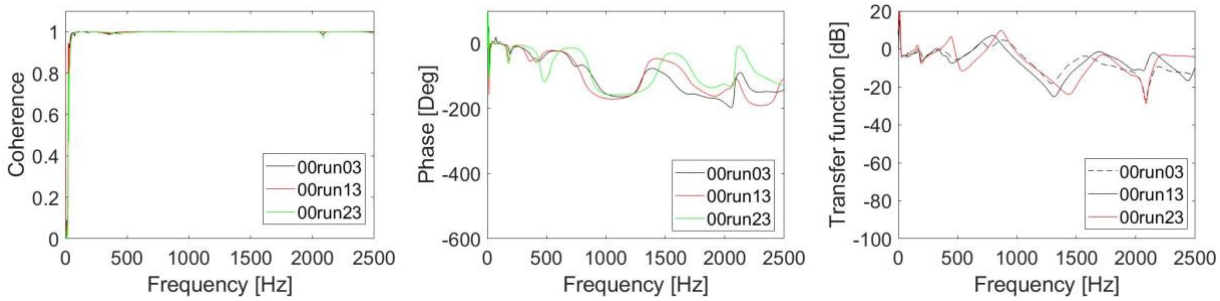

Figure 47. (left to right) Coherence, phase, and transfer function graphs for run 3 of each nonconsecutive set for when sensor III was twisted back to its original position (0 degrees) after being loosened by 15 degrees.

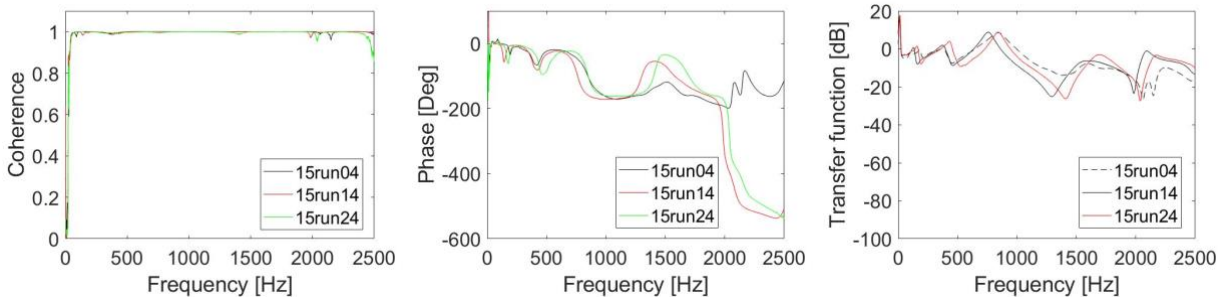

Figure 48. (left to right) Coherence, phase, and transfer function graphs for run 4 of each nonconsecutive set for when sensor III was loosened by 15 degrees for the last time.

Loosened Sensor III Coupling by 30 Degrees

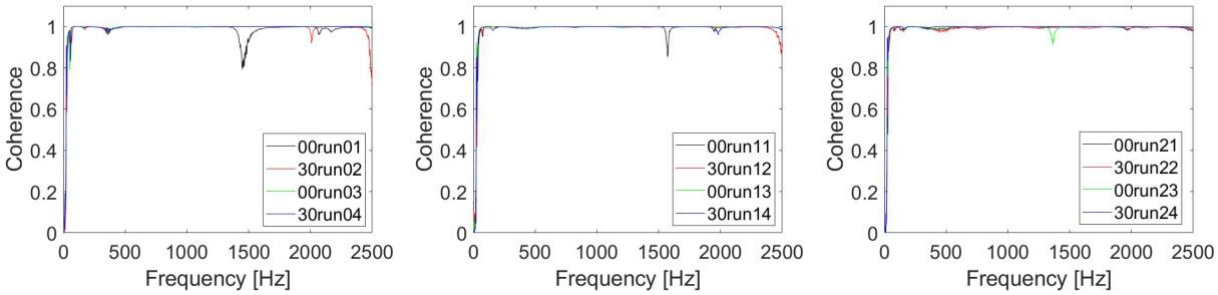

Figure 49. Coherence graphs for loosened sensor III coupling from 0 to 30 degrees within sets 0, 1, and 2.

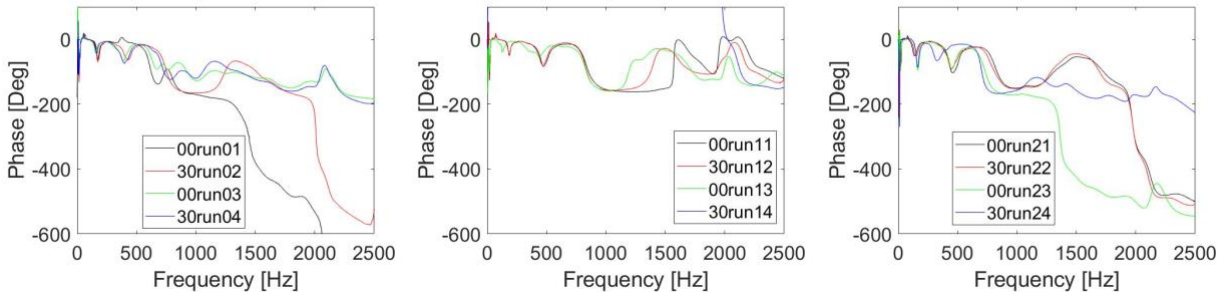

Figure 50. Phase graphs for loosened sensor III coupling from 0 to 15 degrees within sets 0, 1, and 2.

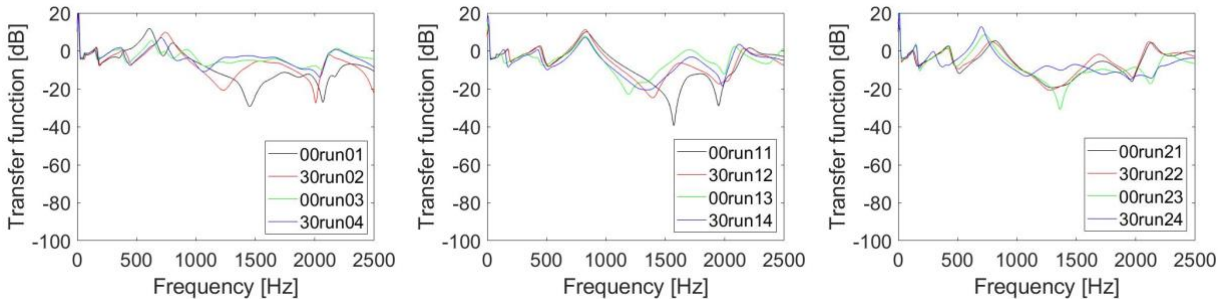

Figure 51. Transfer function graphs for loosened sensor III coupling from 0 to 30 degrees within sets 0, 1, and 2.

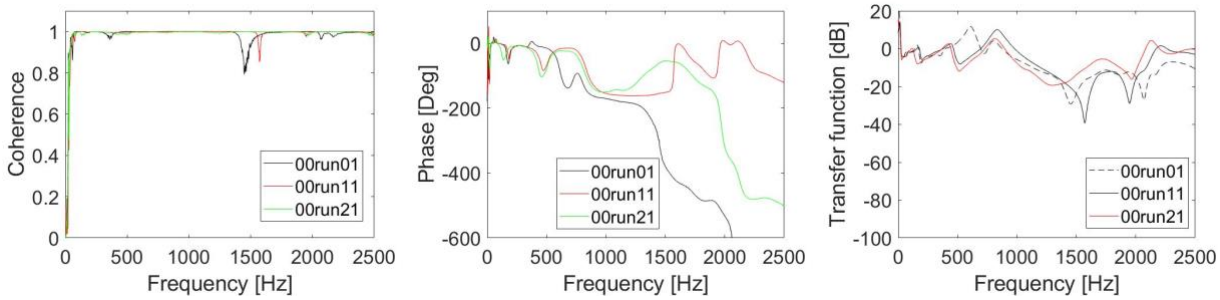

Figure 52. (left to right) Coherence, phase, and transfer function graphs for run 1 of each nonconsecutive set for when sensor III was at its original position (0 degrees) before loosening it by 30 degrees.

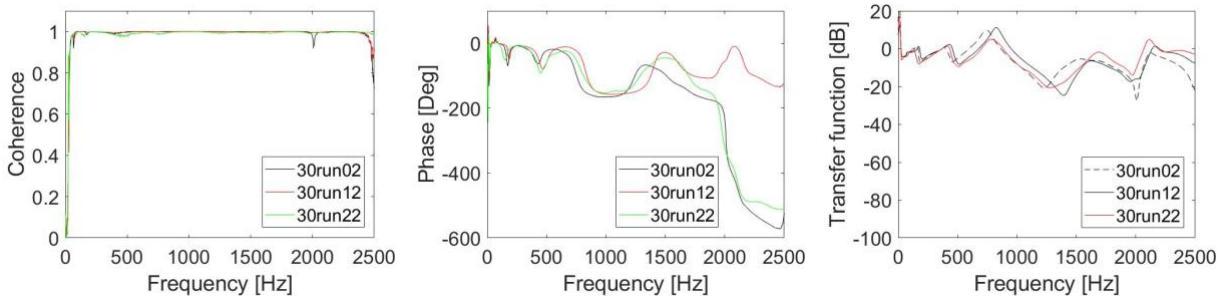

Figure 53. (left to right) Coherence, phase, and transfer function graphs for run 2 of each nonconsecutive set for when sensor III was loosened by 30 degrees for the first time.

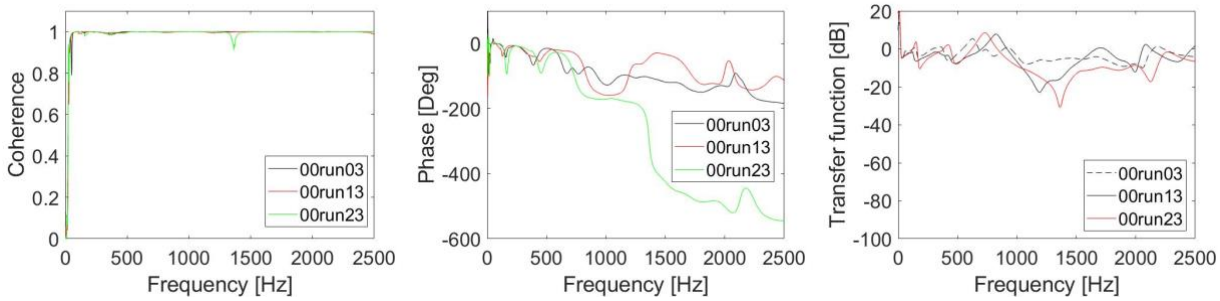

Figure 54. (left to right) Coherence, phase, and transfer function graphs for run 3 of each nonconsecutive set for when sensor III was twisted back to its original position (0 degrees) after being loosened by 30 degrees.

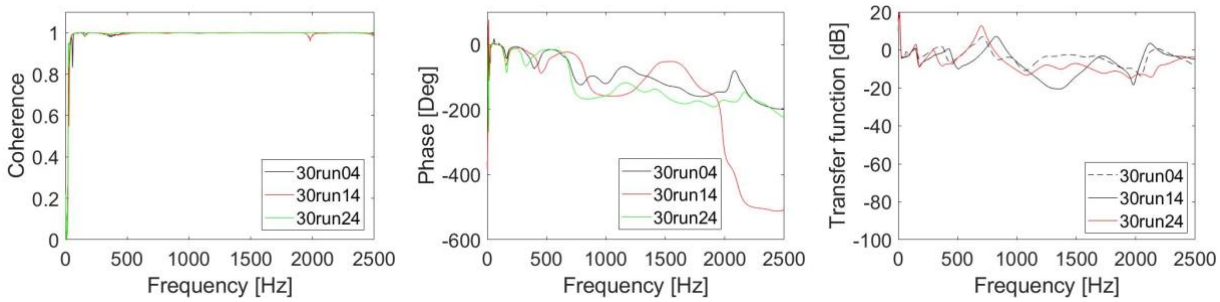

Figure 55. (left to right) Coherence, phase, and transfer function graphs for run 4 of each nonconsecutive set for when sensor III was loosened by 30 degrees for the last time.

Table 4. Quantified Variability of Transfer Functions between Nonconsecutive Sets for Loosened Sensor III Coupling of 15 Degrees

Runs Compared	Average Value of Differences between 50-500 Hz [dB]	Average Value of Differences between 501-1100 Hz [dB]	Average Value of Differences between 1101 – 2000 Hz [dB]
00 degrees - 01, 11, 21	0.342933333	1.7504	3.7121
15 degrees - 02, 12, 22	0.512466667	3.1078	2.6026
00 degrees – 03, 13, 23	1.5702	1.337466667	1.9245
15 degrees – 04, 14, 24	0.9788	2.279333333	1.67

Table 5. Quantified Variability of Transfer Functions between Nonconsecutive Sets for Loosened Sensor III Coupling of 30 Degrees

Runs Compared	Average Value of Differences between 50-500 Hz [dB	Average Value of Differences between 501-1100 Hz [dB]	Average Value of Differences between 1101 – 2000 Hz [dB]
00 degrees - 01, 11, 21	1.0424	3.133533333	2.9864
30 degrees - 02, 12, 22	1.051733333	2.3284	1.4338
00 degrees – 03, 13, 23	1.292333333	0.692133333	5.2285
30 degrees – 04, 14, 24	1.496466667	0.6592	4.8288

4.4 – Analysis and Discussion

In these trials, loosening of the nut on sensor III for the purposes of inducing alterations in coupling ended up causing variation in the transfer function and phase but not the coherence graphs. Not much variability was seen in coherence graphs across nonconsecutive sets and the graphs for the back-to-back trials, but there was indeed variability when it came to the phase and transfer function graphs for nonconsecutive sets. The reason for this was the interference of signal detection accentuated by the loosening of sensor III's nut, which may have made it more difficult for the sensors to obtain precise readings. There was not a significant trend in which runs yielded the most variability within a set, or whether loosening 15 degrees versus 30 degrees made a difference. However, it can be said that there was more variation in the transfer function across nonconsecutive sets between 501-1100 Hz and 1101-2000 Hz as compared to the 50-500 Hz range. This was shown by Tables 4 and 5 which show the average differences between transfer function graphs for a certain numbered run across nonconsecutive sets. This trend is likely due to the presence of a greater signal to noise ratio for higher frequencies that causes variability in data. When this ratio is lower, as seen in the range of 50-500 Hz, there is less

variability between nonconsecutive sets of data. Therefore, the 50-500 Hz range could be optimal for the detection of DDH, but further experimentation needs to be done.

CHAPTER 5: ALTERED VERTICAL FEMUR ALIGNMENT

5.1 – Objective and Hypothesis

The purpose of the experiment was to examine how the tilting of the femur affects the variability in data associated with the coherence, phase, and transfer function graphs made by the MATLAB DDH program. If the angle between the femur and the normal of the exciter surface is increased, the variability of the data will also increase because vertical misalignment will interfere with signal detection between the accelerometers.

5.2 – Methodology

Sensors II and III were calibrated by running the MATLAB DDH Program with sensor III on top of II. After this was run, it was made certain that the saturation of signal was 1 and the time domain was consistent with no settling. When the calibration yielded a coherence value of 1 and a transfer function of 0 dB throughout their respective graphs, the experiment was set in motion. Sensor II was placed face down onto the iLouder exciter surface using only a minimal amount of accelerometer wax, and the patellar notch of the left femur was attached to the back of sensor II using 0.1 g of wax. The center of the left femur was attached to the center of the left acetabulum using 0.2 g of accelerometer wax and the crest of the acetabulum was traced along the exposed femoral head to maintain setup consistency. Sensor III was attached to the nut on top of the iliac crest using 0.1 g of accelerometer wax. None of the sensor wires were taut, but it was confirmed that the sensor wires were not touching before the experiment was run. A protractor was used to make sure that the lateral edge of the femur was aligned at 0 degrees from the normal, and the MATLAB DDH program was run for one set of three back-to-back trials. After

this set, the apparatus was taken apart and put back together to start another set of three back-to-back trials, and this was repeated until three nonconsecutive sets of data were obtained. After this was completed for the 0 degree angle, the femur was tilted 2.5 degrees laterally past the normal of the exciter surface, and the procedure was repeated. After completing the 2.5 degree trials, the femur was tilted 5 degrees laterally past the normal of the exciter surface and three sets of data were once again obtained.

Figure 56. (left to right) Experimental setups for altered vertical femur alignment at 0 degrees, 2.5 degrees, and 5 degrees to the lateral.

5.3 – Data

Vertical Femur Tilt of 0 Degrees

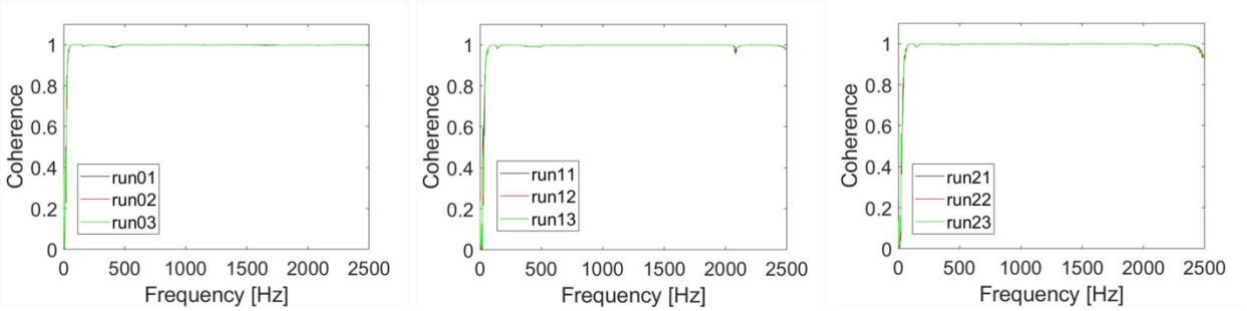

Figure 57. Coherence graphs for back-to-back trials within each set for a vertical tilt of 0 degrees laterally.

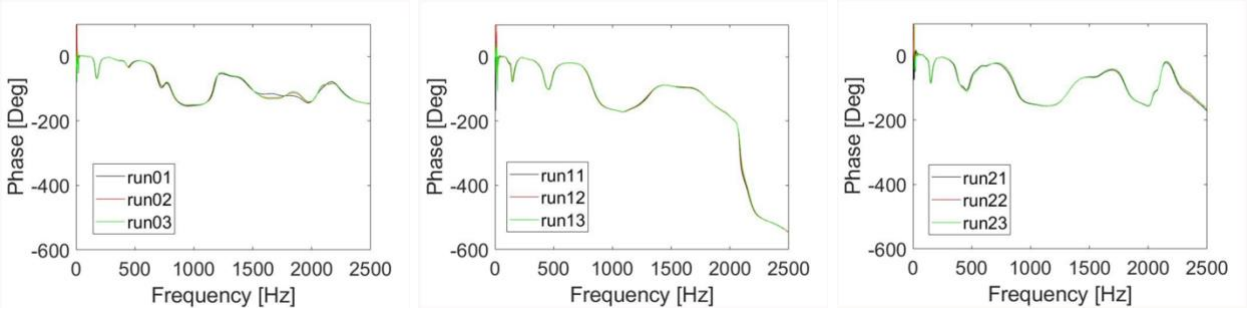

Figure 58. Phase graphs for back-to-back trials within each set for a vertical tilt of 0 degrees laterally.

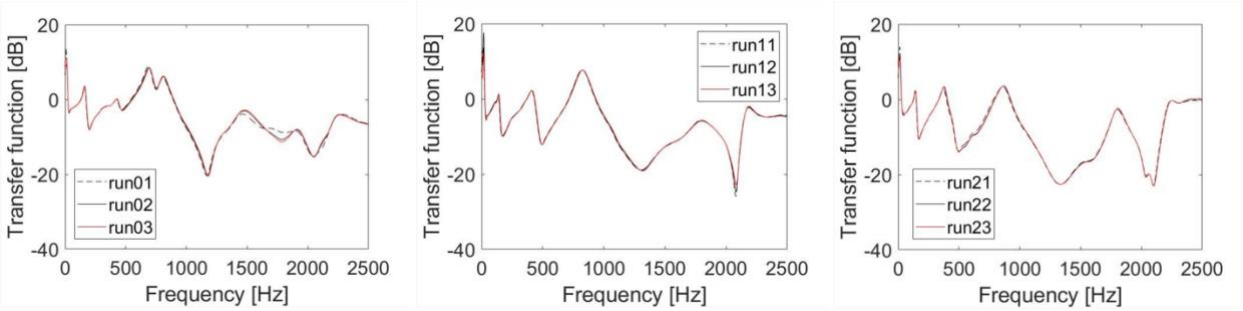

Figure 59. Transfer function graphs for back-to-back trials within each set for a vertical tilt of 0 degrees laterally.

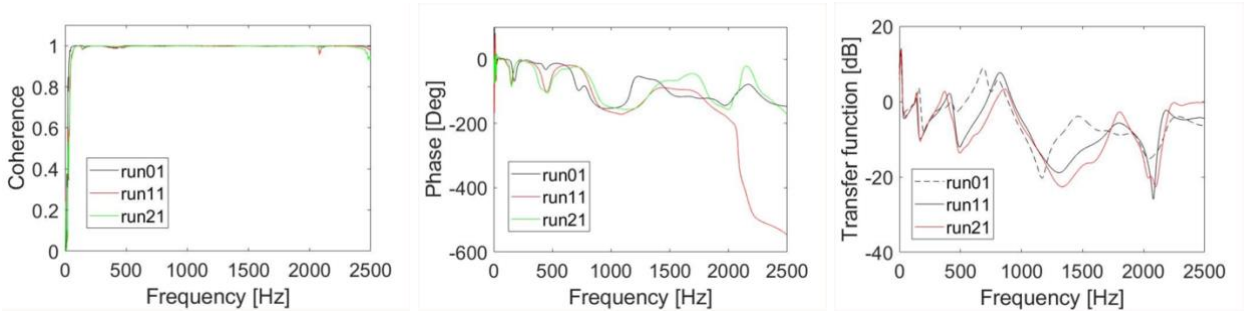

Figure 60. (left to right) Coherence, phase, and transfer function graphs for the first run of each nonconsecutive set for a vertical left femur alignment of 0 degrees to the normal of the exciter surface.

Vertical Femur Tilt of 2.5 Degrees

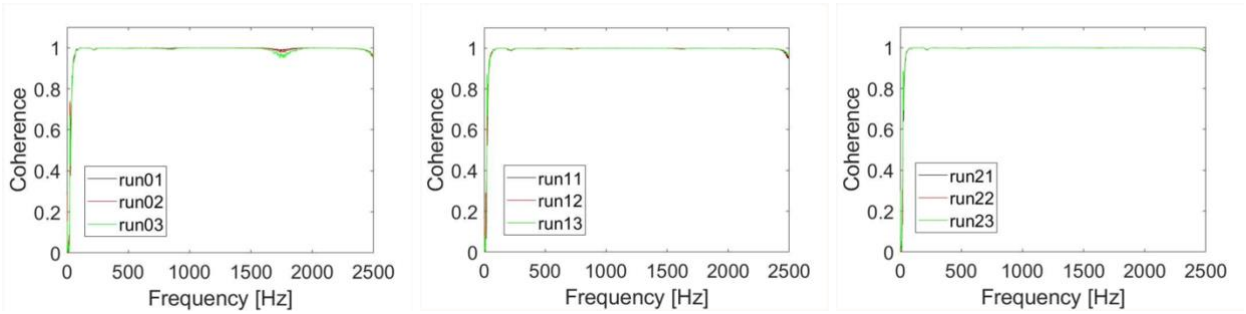

Figure 61. Coherence graphs for back-to-back trials within each set for a vertical tilt of 2.5 degrees laterally.

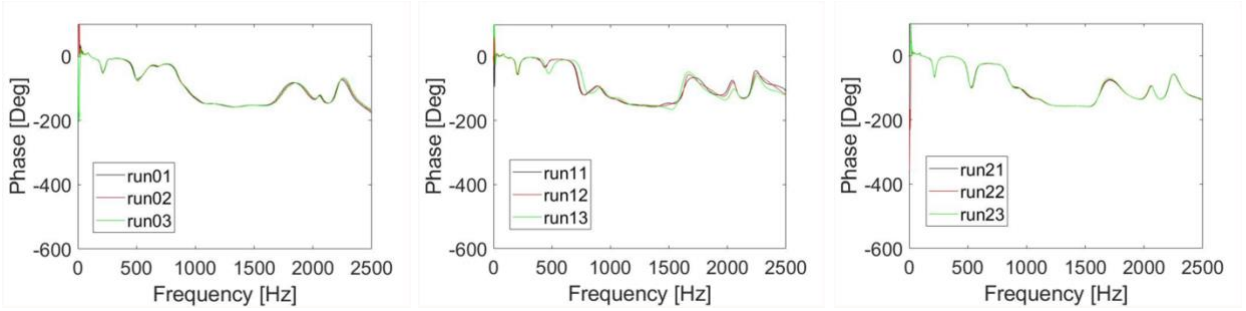

Figure 62. Phase graphs for back-to-back trials within each set for a vertical tilt of 2.5 degrees laterally.

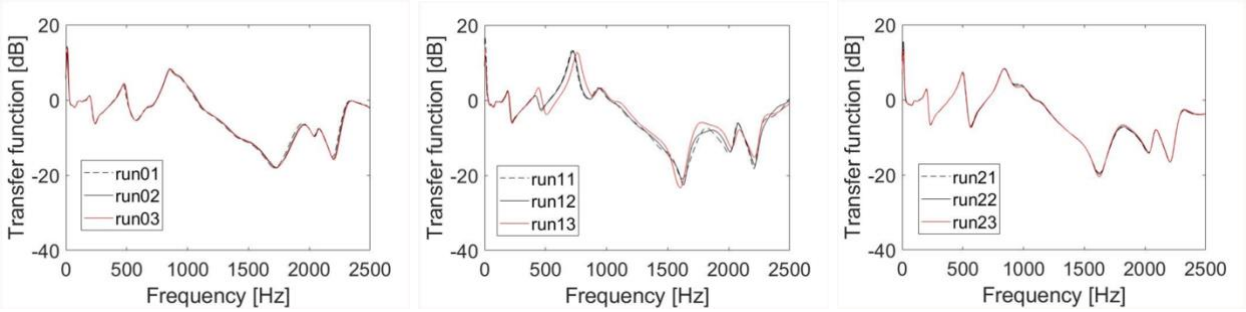

Figure 63. Transfer function graphs for back-to-back trials within each set for a vertical tilt of 2.5 degrees laterally.

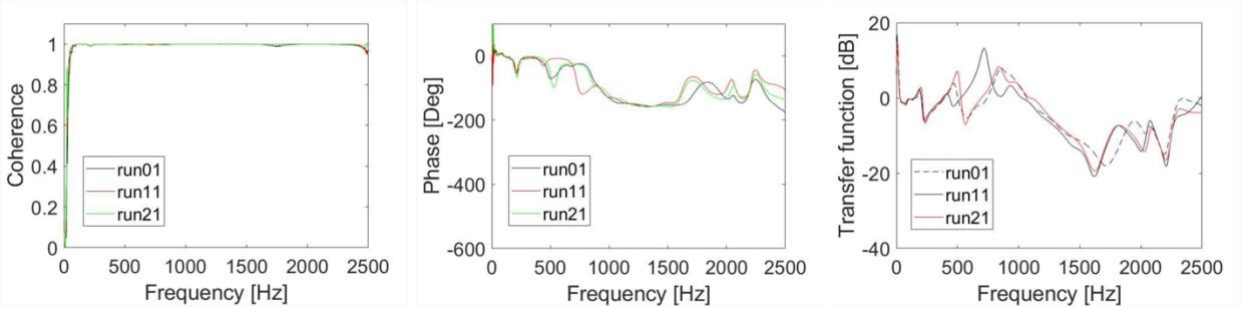

Figure 64. (left to right) Coherence, phase, and transfer function graphs for the first run of each nonconsecutive set for a vertical left femur alignment of 2.5 degrees to the normal of the exciter surface.

Vertical Femur Tilt of 5 Degrees

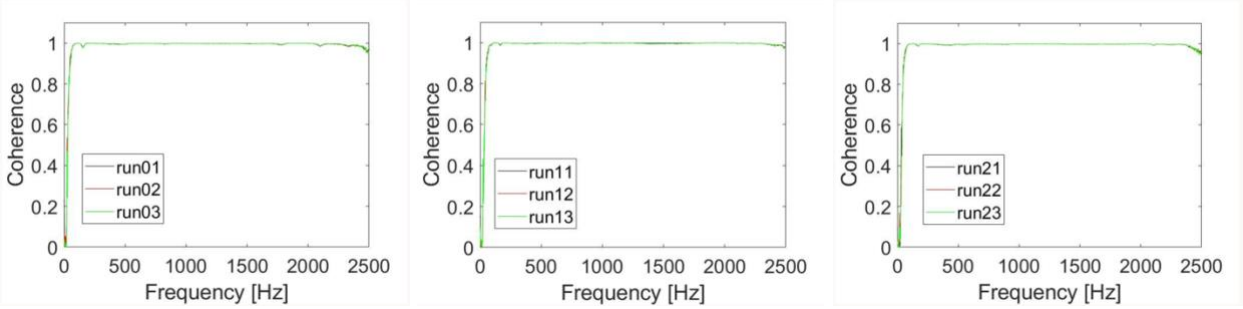

Figure 65. Coherence graphs for back-to-back trials within each set for a vertical tilt of 5 degrees laterally.

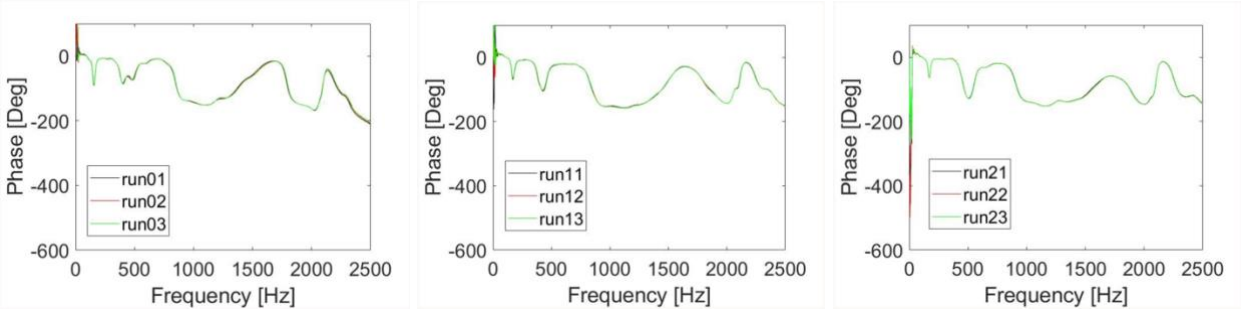

Figure 66. Phase graphs for back-to-back trials within each set for a vertical tilt of 5 degrees laterally.

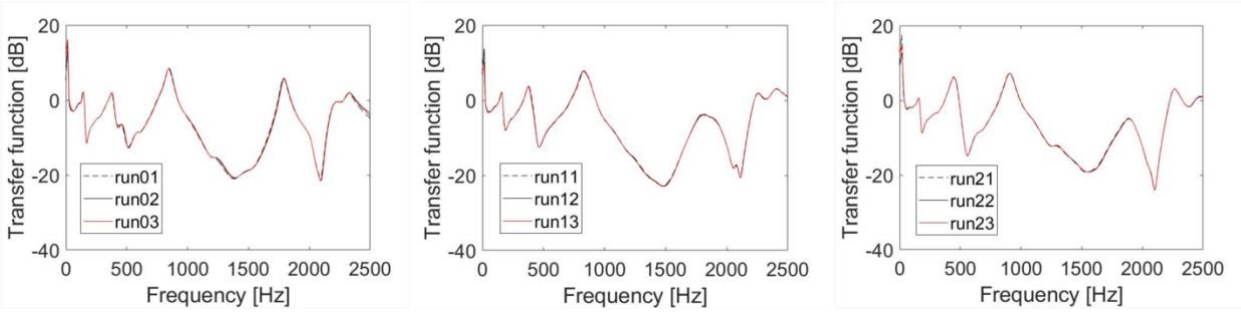

Figure 67. Transfer function graphs for back-to-back trials within each set for a vertical tilt of 5 degrees laterally.

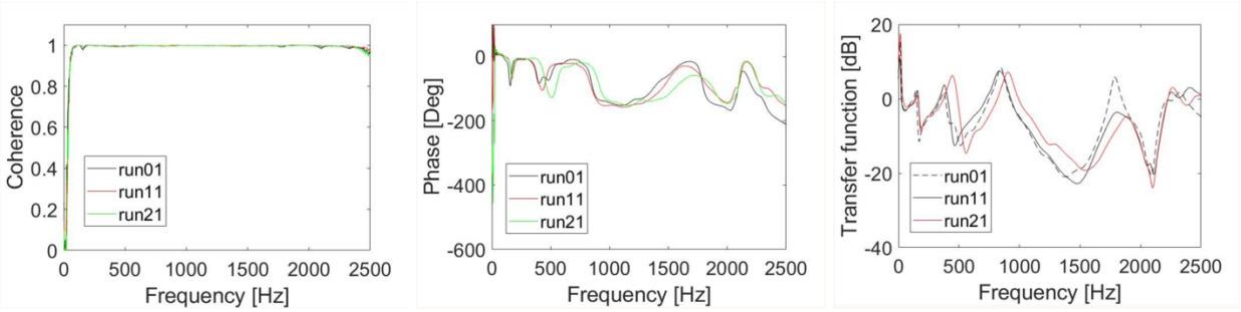

Figure 68. (left to right) Coherence, phase, and transfer function graphs for the first run of each nonconsecutive set for a vertical left femur alignment of 5 degrees to the normal of the exciter surface.

Comparison across Different Vertical Alignment Angles

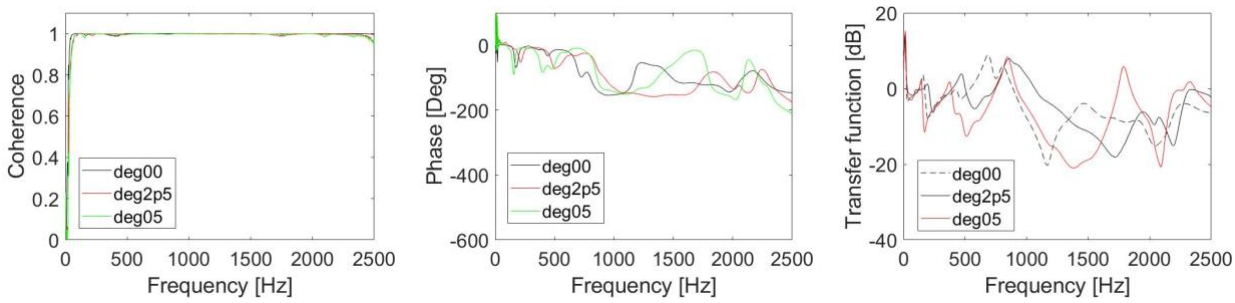

Figure 69. (left to right) Coherence, phase, and transfer function graphs for run 01 of each variation in the lateral tilt of the left femur, including 0 degrees, 2.5 degrees, and 5 degrees from the normal.

Table 6. Quantified Variability of Transfer Functions between Nonconsecutive Sets for Altered Vertical Femur Tilt

Runs Compared	Average Value of Differences between 50-500 Hz [dB]	Average Value of Differences between 501-1100 Hz [dB]	Average Value of Differences between 1101 – 2000 Hz [dB]
Tilt of 0.0 degrees – 01, 11, 21	1.125533333	3.260933333	3.1842
Tilt of 2.5 degrees – 01, 11, 21	0.631133333	1.363266667	0.887
Tilt of 5.0 degrees – 01, 11, 21	1.837066667	0.9826	1.3039

5.4 – Analysis and Discussion

The tilting of the femur of the 3D printed bone apparatus resulted in an interesting trend. The back-to-back trials all were very consistent and repeatable in terms of coherence, phase, and transfer function no matter how far the femur was tilted. However, the data from the nonconsecutive trials told a different story and did not seem to have a pattern either. It was predicted that tilting the femur more would result in a greater degree of variation across the first runs of nonconsecutive sets, but this is not seen in Table 6. Astoundingly, the tilt of 2.5 degrees produced a lower average difference than the 0.0 and 5.0 degree tilts in the 50-500 Hz and 1100-

2000 Hz ranges. The opposite trend from what was hypothesized was seen in the 501-1100 Hz range since the increased tilt of the apparatus correlated with a lower average difference between the first runs of each nonconsecutive sets. Despite these fluctuations from the expectations, it is still displayed that the range of average differences between nonconsecutive sets is the lowest in the 50-500 Hz range, the second lowest in the 501-1100 Hz range, and the highest in the 1100-2000 Hz range. Although the tilt of the femur did not yield the hypothesized results, it can be affirmed that 50-500 Hz frequencies could be optimal in the detection of DDH in infants based on the results of the 3D printed bone model as the variability of the transfer function graphs in this range was relatively close to 1 dB.

CHAPTER 6: PRELIMINARY TESTING USING A RAW CHICKEN QUARTER

6.1- Objective and Hypothesis

The purpose of the experiment is to see how the chicken knee joint behaves when an excitation signal is sent through the knee joint in terms of variation in the transfer function, phase, and coherence graphs as sensed by accelerometers placed on the femoral head and the articular (bottom) surface of the tibia. If the chicken quarter is stabilized and run through back-to-back and nonconsecutive trials, then the coherence, phase, and transfer function graphs should be the same if not similar because the soft tissue introduced in the experiment should not drastically affect the transmission of the excitation signal between the two accelerometers.

6.2 – Methodology

The chicken leg quarter was dissected using a scalpel, forceps and a set of surgical scissors to remove the fragments of the pelvic bone and acetabulum so that the femoral head could be accessed. The head of the raw chicken femur was fully exposed and cleaned off so that a small nut could be superglued onto the center of the femoral head. The remnants of the Achilles tendon and the foot were cut off the bottom part of the chicken quarter. The bottom bulge of the tibia was exposed so the articular surface could be cleaned, and another nut was superglued onto this surface. While the glue dried, sensor II and III were calibrated to make sure the time domain was consistent, the initial coherence was 1 unit, and the transfer function was 0 dB throughout the graph. The chicken leg quarter was placed on a plastic tray covered with a couple layers of paper towels with the femoral head facing upward and the articular surface

facing the experimenters. Sensor III was attached to the nut on the femoral head using 0.2 g of accelerometer wax, and the back of sensor II was attached to the nut on the articular surface using 0.2 g of wax. An iLouder exciter was placed on its side on a block of foam, and adjusted so that sensor II could attach to it using 0.1 g of accelerometer wax. Using the MATLAB DDH detection program, a set of three back-to-back trials were run to comprise one set of data. Two more nonconsecutive sets were run like this, separated by the removal and replacement of the sensors on their respective nuts.

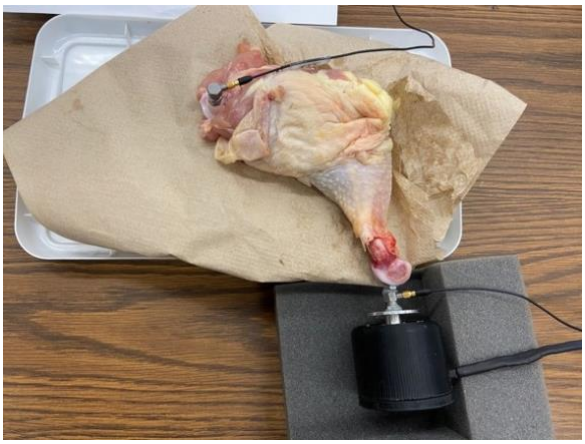

Figure 70. Experimental setup for preliminary raw chicken leg quarter trials. This was kept consistent throughout the experiment, even across nonconsecutive sets.

6.3 – Data

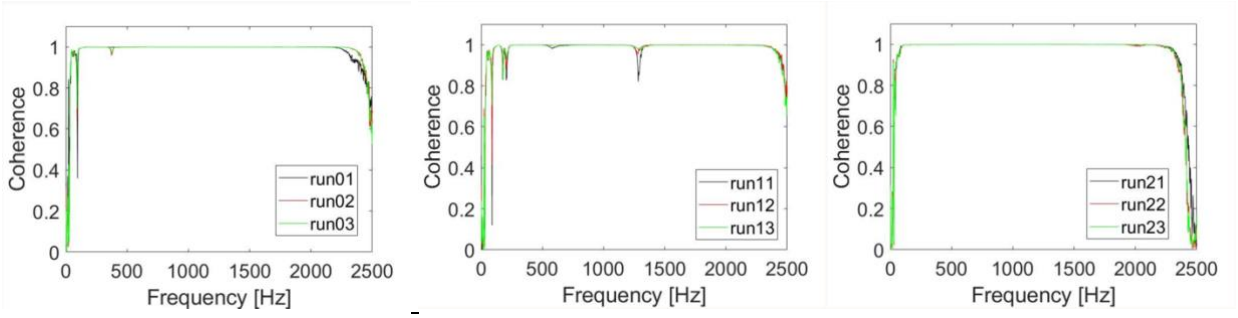

Figure 71. Coherence graphs for back-to-back trials within each set for the preliminary chicken leg quarter trials.

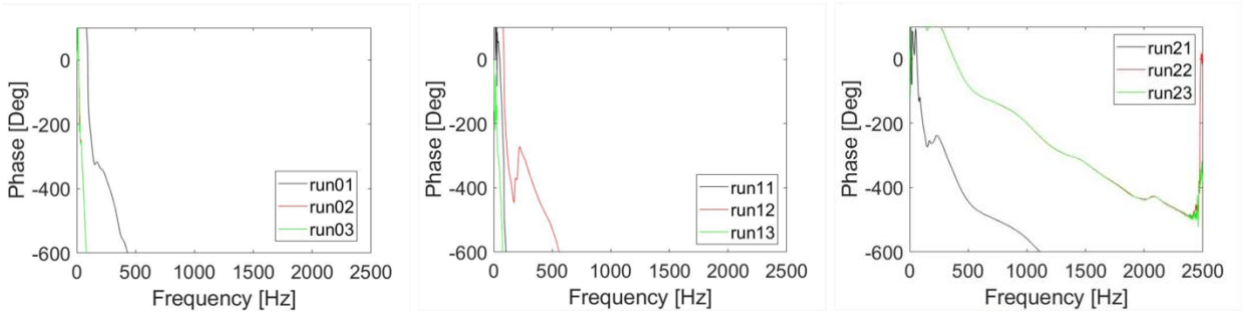

Figure 72. Phase graphs for back-to-back trials within each set for the preliminary chicken leg quarter trials.

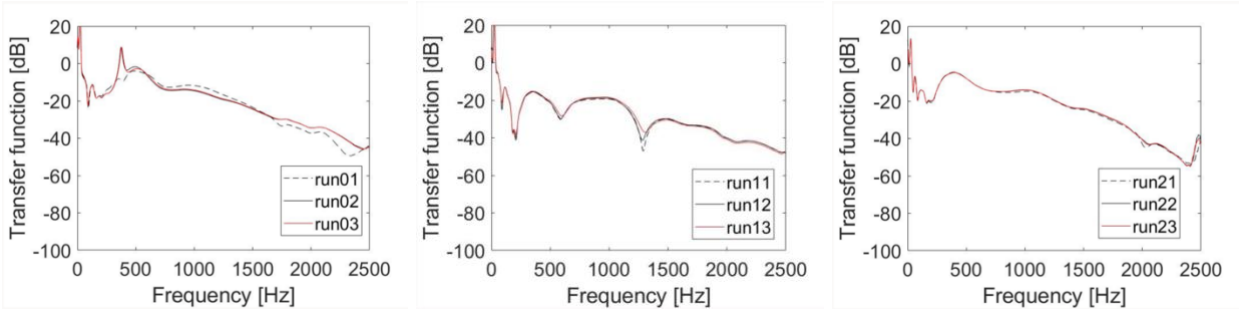

Figure 73. Transfer function graphs for back-to-back trials within each set for the preliminary chicken leg quarter trials.

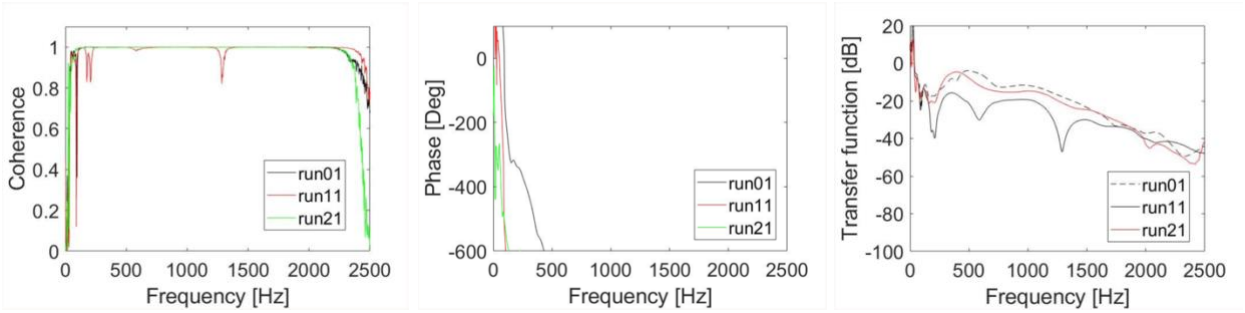

Figure 74. (left to right) Coherence, phase, and transfer function graphs for the first run of each nonconsecutive set for the preliminary chicken leg quarter trials.

Table 7. Quantified Variability of Transfer Functions between Nonconsecutive Sets for Preliminary Chicken Trials

Runs Compared	Average Value of Differences between 50-500 Hz [dB]	Average Value of Differences between 501-1100 Hz [dB]	Average Value of Differences between 1101 – 2000 Hz [dB]
Intact Knee – 01, 11, 21	6.072066667	7.679266667	5.222066667

6.4 - Analysis and Discussion

This was the first time that the study involved an animal specimen for the purposes of variability testing. The introduction of soft tissue when it came to testing the iLouder exciter and the used accelerometers was expected to give different results, but it was not certain how much variation that soft tissue would introduce. The coherence and transfer function graphs for the preliminary chicken trials were very consistent for back-to-back trials within one set, but the same could not be said for phase. Phase graphs exhibited a very different pattern than what was seen in those of the 3D printed bone model. The nonconsecutive sets of coherence data were very consistent with one another, but when it came to transfer function, there was quite a bit of variability. This is especially demonstrated in Table 7 where average differences in transfer function values across all frequency ranges are greater than 5 dB. It is uncertain whether this is due to the introduction of soft tissue or another confounding variable. However, the transfer function seems more similar between runs 01 and 21 while run 11 differed significantly. This could have skewed the average difference value by itself, even though runs 11, 12, and 13 showed consistent transfer function data in Figure 71. Further experimentation must be conducted with this data, but because the back to back trials were consistent, the ability to obtain repeatable data should not be discounted.

CHAPTER 7: DISLOCATION OF A RAW CHICKEN KNEE JOINT

7.1 – Objective and Hypothesis

The purpose of the experiment is to examine the influence of different degrees of chicken knee joint dislocation on the data collected on coherence, phase, and transfer function as sensed by accelerometers placed on the head of the raw chicken femur and the articular (bottom) surface of its tibia. If the chicken knee joint is increasingly dislocated, then this will lead to significant changes in coherence, phase, and transfer function data as the signal detection between the two sensors will be increasingly interrupted as the degree of dislocation becomes more drastic.

7.2 – Methodology

A raw chicken leg quarter was positioned on a paper towel covered plastic tray with the femoral head facing toward the ceiling and the articular surface of the tibia facing toward the experimenters. A scalpel, forceps, and a set of surgical scissors were used to remove pelvic bone fragments as well as what was left of the hip joint of the chicken for the purpose of exposing the femoral head of the chicken quarter. Once the ligaments and non-bone tissue were cleaned off the femur head, a small nut was glued onto the center. After this, the chicken's Achilles tendon was severed as well as the remnants of the chicken foot. This exposed the articular surface of the chicken tibia so that another nut could be glued onto this portion. As the glue took time to set and dry, sensors II and III were calibrated with the iLouder exciter to ensure a consistent time domain, a starting coherence of 1 unit, and a transfer function of 0 dB throughout the graphs. 0.2 g of accelerometer wax was used to attach the nut of sensor III onto the head on the femur. Another 0.2 g of accelerometer wax was used to place back of sensor II onto the articular

surface, and 0.1 g of accelerometer wax attached the nut of sensor II onto the surface of the iLouder exciter which was placed on its side on a block of foam. For the first part of the experiment, the chicken knee was kept intact while the MATLAB DDH detection was run three nonconsecutive sets of three back-to-back trials each. Nonconsecutive sets were distinguished by the removal and replacement of sensors on the chicken between each set. The same pattern of sets and trials was repeated for three different cases as well: the partial dislocation, the foam separation, and complete dislocation of the chicken quarter knee joint. Partial dislocation involved exposing the chicken knee and severing some of the anterior ligaments holding the femur to the tibia, but keeping the knee together and touching. Foam separation entailed cutting a couple more ligaments on the side and in the middle of the knee and inserting a small piece of foam in the middle of the knee joint. Finally, complete dislocation included severance of all ligaments of the knee and separation of the tibia and the femur by approximately half an inch of air.

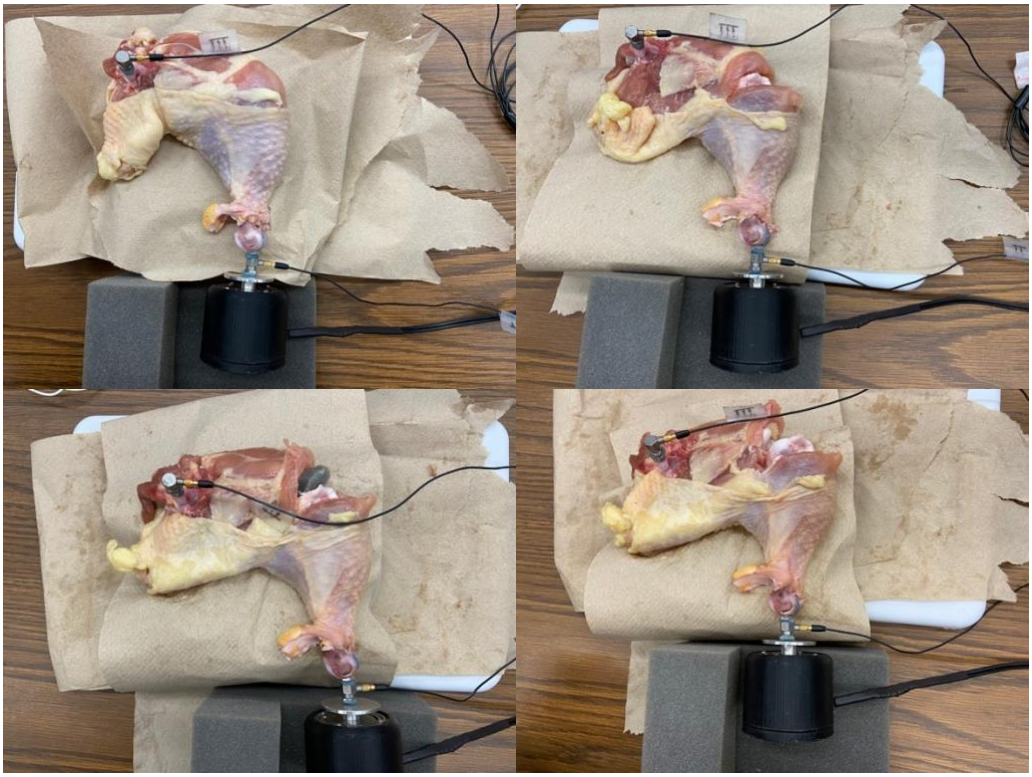

Figure 75. Experimental set ups for chicken dislocation trials. The intact (top left), partially dislocated (top right), foam separated (bottom left), and completely dislocated (bottom right) knees are shown.

7.3 – Data

Intact Chicken Knee

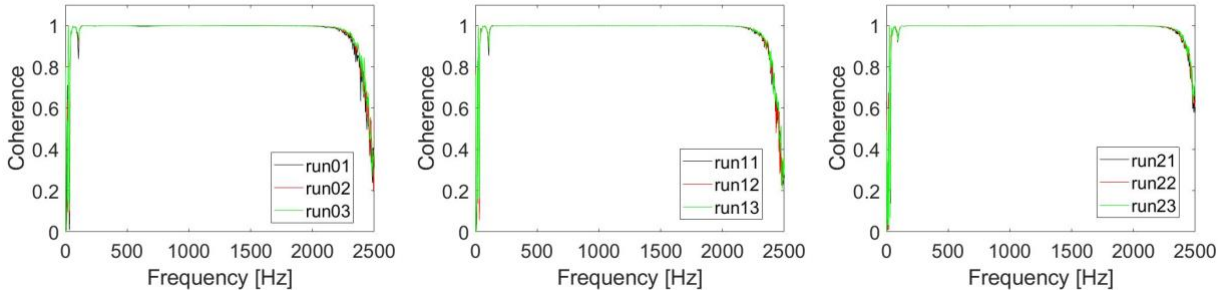

Figure 76. Coherence graphs for back-to-back trials within each set for the intact chicken knee.

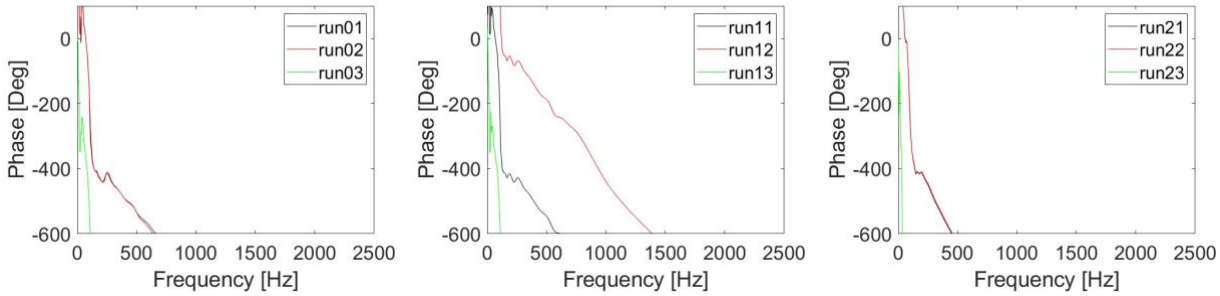

Figure 77. Phase graphs for back-to-back trials within each set for the intact chicken knee.

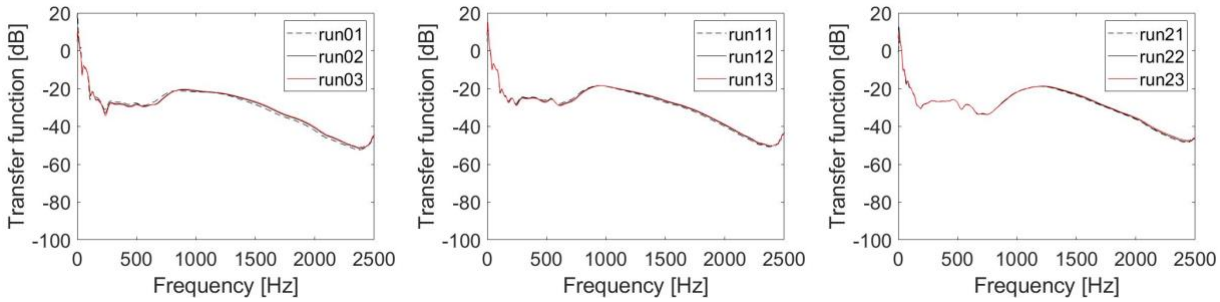

Figure 78. Transfer function graphs for back-to-back trials within each set for the intact chicken knee.

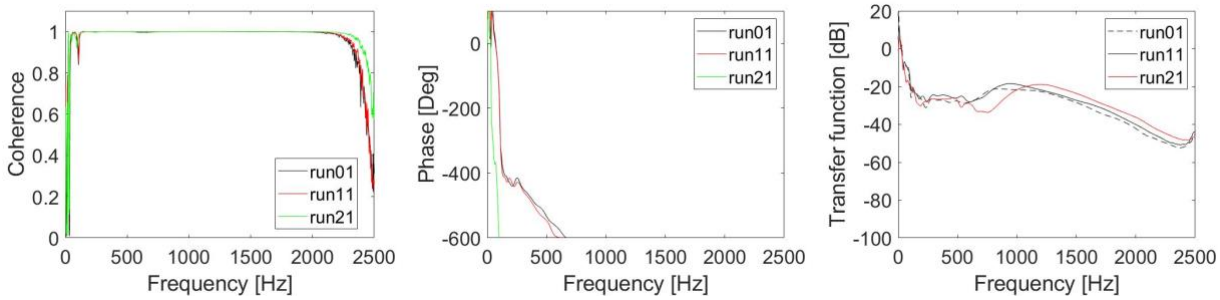

Figure 79. Coherence, phase, and transfer function graphs for the first run of each nonconsecutive set for the intact chicken knee trials.

Partially Dislocated Chicken Knee

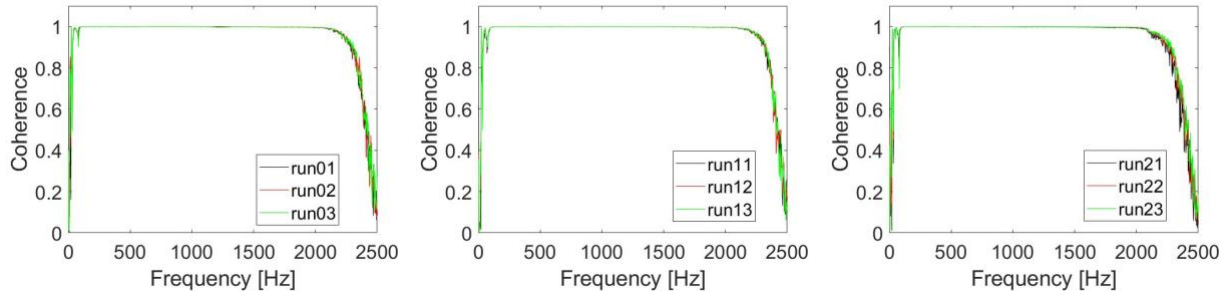

Figure 80. Coherence graphs for back-to-back trials within each set for the partially dislocated chicken knee.

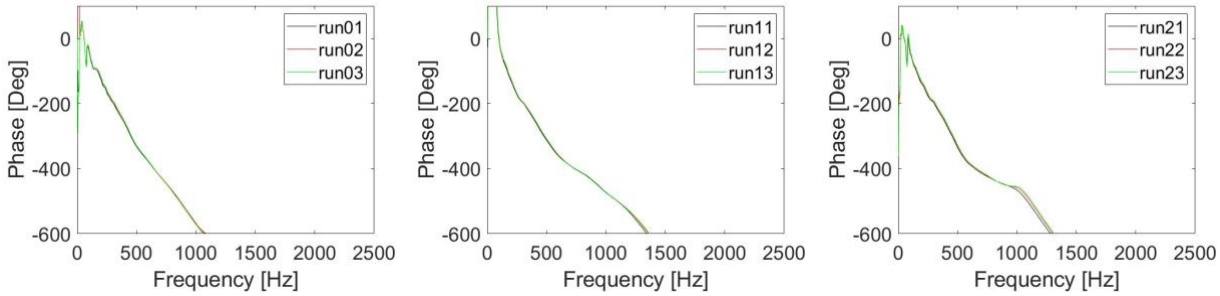

Figure 81. Phase graphs for back-to-back trials within each set for the partially dislocated chicken knee.

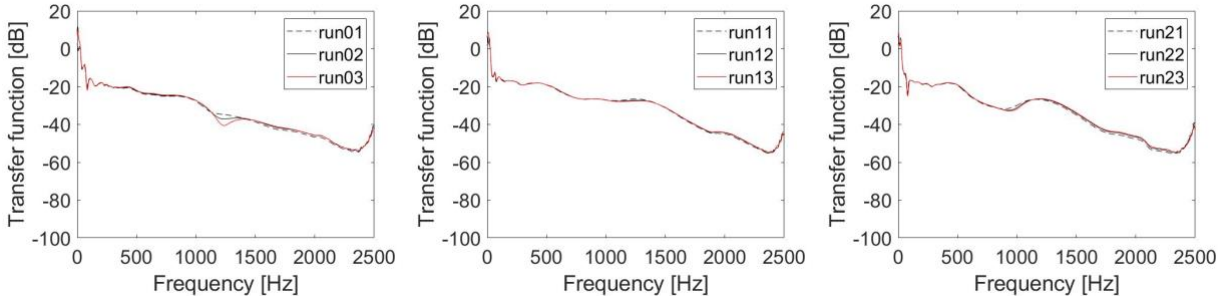

Figure 82. Transfer function graphs for back-to-back trials within each set for the partially dislocated chicken knee.

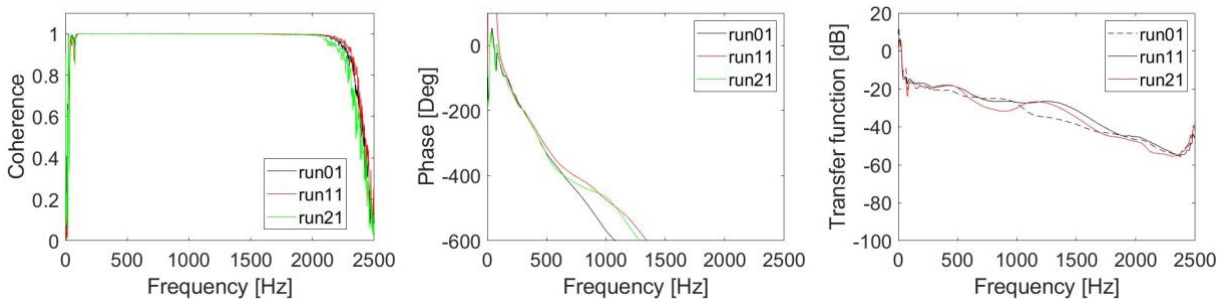

Figure 83. (left to right) Coherence, phase, and transfer function graphs for the first run of each nonconsecutive set for the partially dislocated chicken knee trials.

Foam Separated Chicken Knee

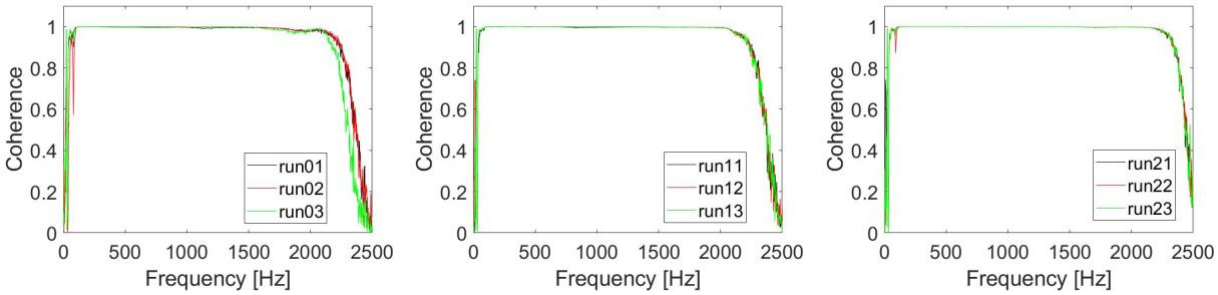

Figure 84. Coherence graphs for back-to-back trials within each set for the foam separated chicken knee.

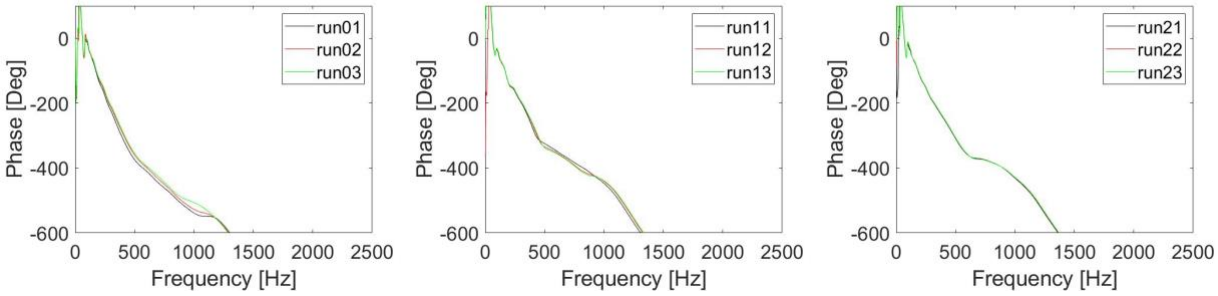

Figure 85. Phase graphs for back-to-back trials within each set for the foam separated chicken knee.

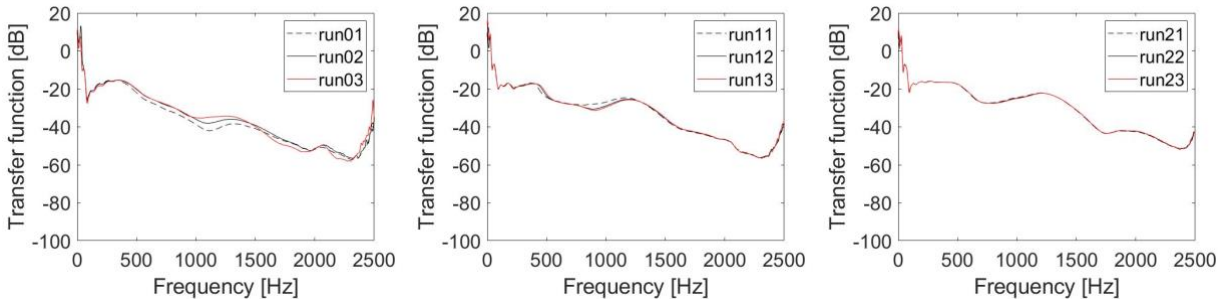

Figure 86. Transfer function graphs for back-to-back trials within each set for the foam separated chicken knee.

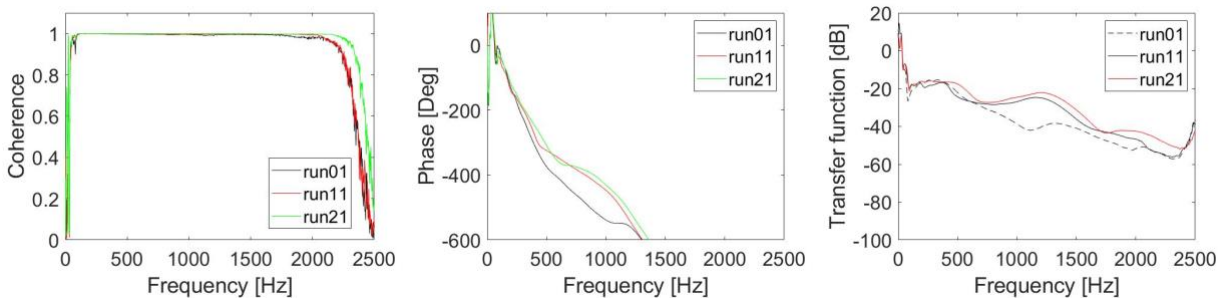

Figure 87. (left to right) Coherence, phase, and transfer function graphs for the first run of each nonconsecutive set for the foam separated chicken knee trials.

Completely Dislocated Chicken Knee

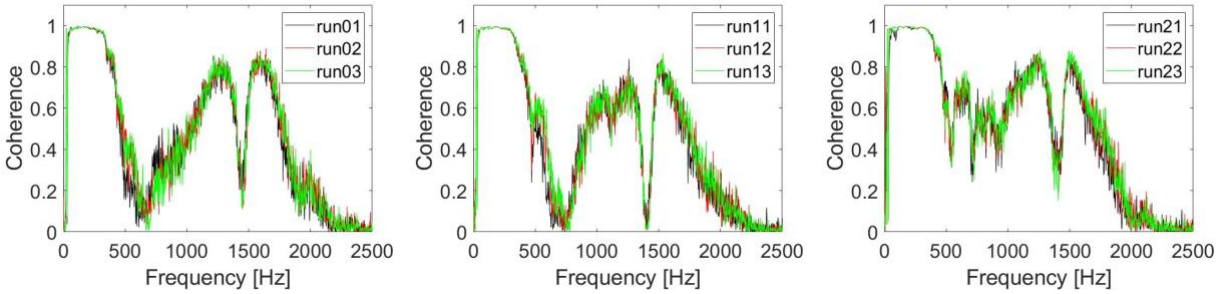

Figure 88. Coherence graphs for back-to-back trials within each set for the completely dislocated chicken knee.

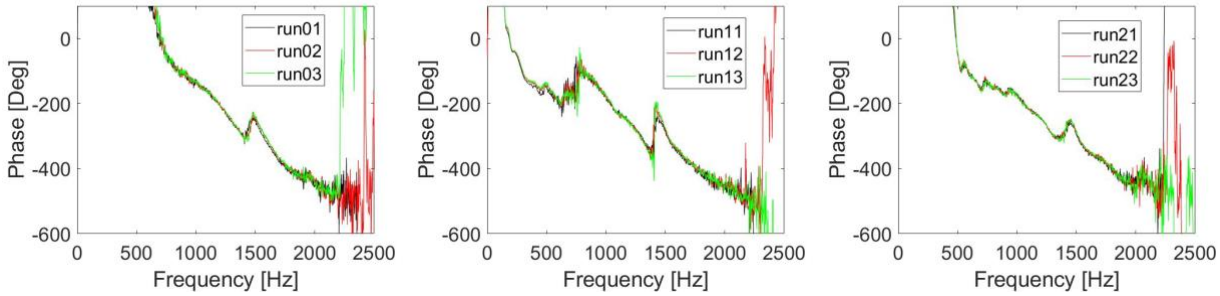

Figure 89. Phase graphs for back-to-back trials within each set for the completely dislocated chicken knee.

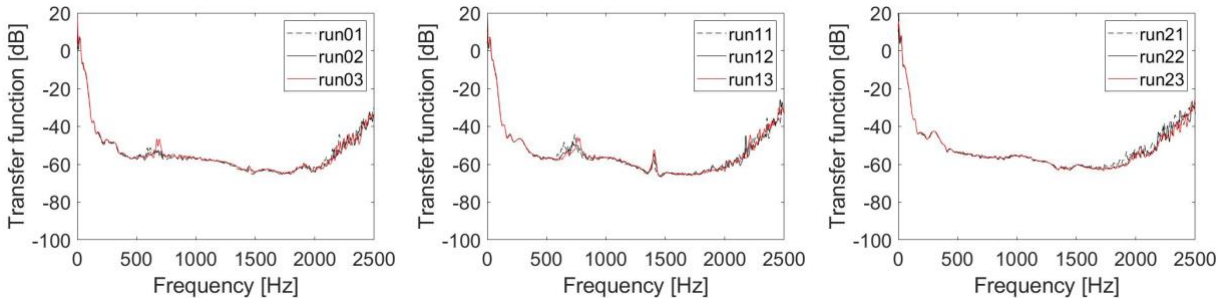

Figure 90. Transfer function graphs for back-to-back trials within each set for the completely dislocated chicken knee.

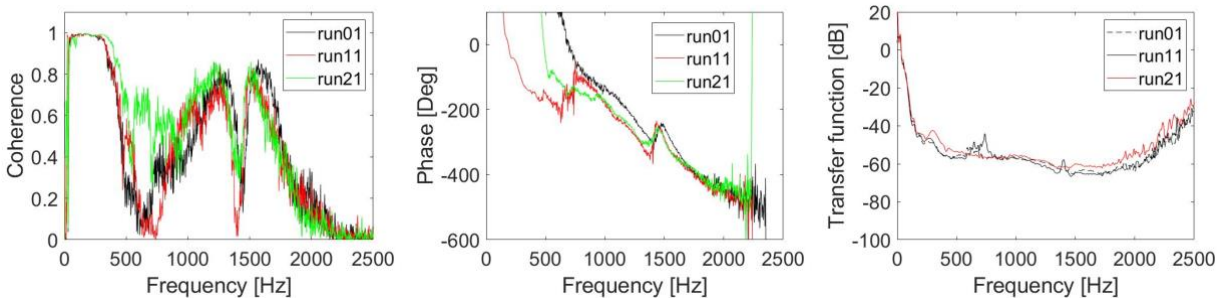

Figure 91. (left to right) Coherence, phase, and transfer function graphs for the first run of each nonconsecutive set for the completely dislocated chicken knee trials.

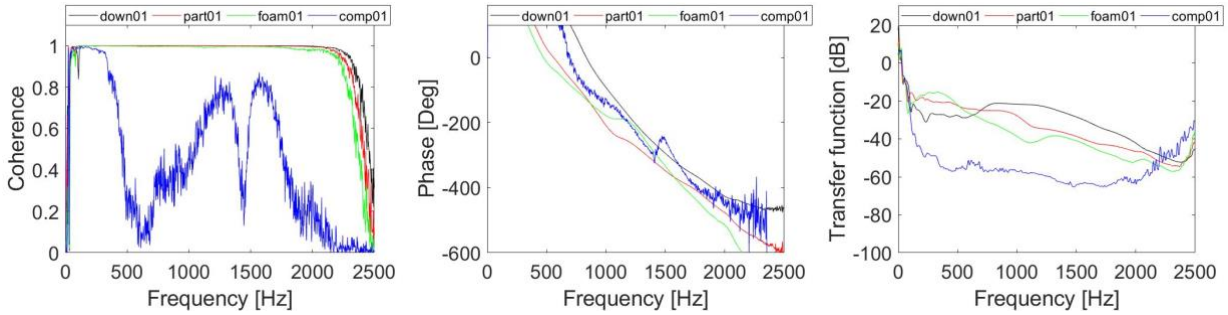

Figure 92. (left to right) Coherence, phase, and transfer function graphs for the first run of each of the cases among the intact, partially dislocated, foam separated, and completely dislocated chicken knees.

Table 8. Quantified Variability of Transfer Functions between Nonconsecutive Sets for Different Degrees of Chicken Knee Dislocation

Runs Compared	Average Value of Differences between 50-500 Hz [dB]	Average Value of Differences between 501-1100 Hz [dB]	Average Value of Differences between 1101 – 2000 Hz [dB]
Intact Knee – 01, 11, 21	1.4596	3.5683	3.130066667
Partial Dislocation – 01, 11, 21	1.118733333	2.101733333	3.497133333
Foam Separation – 01, 11, 21	1.212566667	5.1338	7.037366667
Complete Dislocation – 01,11, 21	2.136133333	0.5097	2.362533333

Table 9. Average Transfer Function Values (Run 01) for Different Degrees of Chicken Knee Dislocation

Cases	Average Value between 50-500 Hz [dB]	Average Value between 501-1100 Hz [dB]	Average Value between 1101 – 2000 Hz [dB]
Intact Knee	-24.622567	-24.74083333	-28.2797
Partial Dislocation	-18.43263333	-26.44606667	-37.07093333
Foam Separation	-17.39756667	-28.13463333	-37.93863333
Complete Dislocation	-44.4001	-55.60263333	-61.7395

Table 10. Average Differences in Transfer Function (Run 01) between the Intact Knee and Different Dysplasias

Cases Compared	Average Difference between 50-500 Hz [dB]	Average Difference between 501-1100 Hz [dB]	Average Difference between 1101 – 2000 Hz [dB]
Intact Knee vs. Partial Dislocation	6.189933333	1.705233333	8.791233333
Intact Knee vs. Foam Separation	7.225	3.3938	9.658933333
Intact Knee vs. Complete Dislocation	19.77753333	30.8618	33.4598

7.4 – Analysis and Discussion

After the preliminary trials with the chicken quarter as seen in chapter 6, it was observed that relatively consistent back to back trials and fairly similar nonconsecutive sets of data could be obtained. The next step was to gradually and intentionally introduce separation of the knee in four different cases: the intact chicken knee, the partially dislocated chicken knee, the foam separated chicken knee, and the completely dislocated chicken knee. With the intact chicken knee, it was observed phase graphs were not consistent among back-to-back trials nor among graphs across the nonconsecutive sets of data. However, the main focus was on the transfer function and coherence graphs as it was assumed that these would give us the most insight. The coherence and transfer function graphs for back-to-back trials and nonconsecutive sets of data was fairly similar if not identical (as seen in back to back trials). This indicates that the results obtained were repeatable and the details of these graphs could be used to signify an intact joint. This was different for what was observed for the preliminary chicken trials in chapter 6 since those transfer functions varied by over 5 dB whereas these values usually varied by 1-2 dB (Table 8).

When some of the ligaments at the knee joint were severed in the case of partial dislocation, this induced the first gradual separation of the joint. Interestingly, the coherence, phase, and transfer function graphs were similar across both back-to-back and nonconsecutive sets, which could not be said for the intact joint. This case was particularly important because it was established that this may be the most similar to the infant hip dislocation cases seen in clinical settings, and the fact that the results were relatively repeatable is promising. Next, the foam separation of the chicken knee was done to see if the porous material of the foam would

simulate the attachment of ligaments even though some ligaments had been severed in the joint. Although the back-to-back and nonconsecutive data was still very consistent and similar across trials, the data from the foam-separated chicken knee looked more similar to that of the partially dislocated chicken knee as compared to the intact knee. Last but certainly not least, the complete dislocation of the chicken knee rendered extremely different results than those seen in the previously run cases. Instead of the coherence being 1 unit throughout most of the graph, the complete dislocation of the knee correlated with a spiky appearance of the coherence graph among back-to-back and nonconsecutive sets of data. There was a dip at 500 Hz and a sharp drop at 1450 Hz across all coherence data for this case. Phase graphs for the complete dislocation case were also a lot less smooth as compared to the previously run cases.

While the transfer functions of the intact chicken knee, the partially dislocated chicken knee, and the foam separated chicken knee gradually decreased across the range presented in their graphs, the completely dislocated knee sharply dropped at 50 Hz and plateaued downward until it rose again around 2000 Hz. In general, the appearances of the graphs for the completely dislocated knee were a lot different from those of the intact, partially dislocated, and foam separated knee.

A similar trend seen in the transfer function quantified variability for the 3D bone experiments was observed in the nonconsecutive data across a single dislocation case in the chicken knee. Variability was around 1 dB for the 50-500 Hz range, about 2-3 dB for the 501-1100 Hz range, and a little higher than 3 dB for the 1101-2000 Hz range (Table 8). This further confirmed that the 50-500 Hz range may be optimal for detecting joint dislocation.

As demonstrated by Table 9, the intact chicken knee had a transfer function around -24 to -28 dB throughout the graph seen in Figure 92. The simulation of ligaments by the foam proved useful since the transfer function values for the partially dislocated knee and the foam separated knee were very similar across all frequency ranges (Table 9). Lastly, there was a drastic dip in transfer function across the entire graph for the completely dislocated case, considering the highest value was -44 dB. Table 9 indicates that the transfer function values for a completely dislocated knee are drastically different than those of intact knee, partial dislocation, or foam separation cases.

To confirm that this experiment indicated dislocation of the chicken knee, the average value of transfer functions across different frequency ranges for the first case of the dislocation trials was compared the value of the intact knee. While the cases for foam separation and partial dislocation differed from the intact knee by 6-7 dB between 50-500 Hz and 8-9 dB between 1101-2000 Hz, they only differed by 1-2 dB between 501-1100 Hz (Table 10). However, since 50-500 Hz seems the most optimal for testing joint dysplasia, this is promising considering the variability between nonconsecutive sets of the same case were only around 1-2 dB. What is interesting is that the complete dislocation of the knee differed around 20-30 dB from the intact knee, which is drastically greater than any nonconsecutive variability obtained in this study. It is probable that this method can be used in the future to differentiate complete dislocation from an intact joint, but this must be explored further.

CHAPTER 8: CONCLUSIONS AND FURTHER EXPERIMENTATION

Throughout the entire set of experiments for the 3D printed bones, it was seen that back-to-back trials of data were consistent and very similar across coherence, phase and transfer function graphs. This was true for the altered wire suspension, loosened sensor II coupling, loosened sensor III coupling, and altered vertical femur tilt experiments. The nonconsecutive sets of data were not as similar across the same graphs, but when variability was quantified for the nonconsecutive transfer function graphs, the data between the 50-500 Hz range only had around 1 dB of variability whereas the data between the 501-1100 Hz range and the 1101-2000 Hz range contained a lot more variation. This indicated that no matter the induced types of variability in the different experiments, the 50-500 Hz range was optimal for the detection of the signal through the acetabular joint as sensed by the accelerometers placed on the patellar notch and the iliac crest, respectively. The relatively low variation in data sets seen in each of these experiments allowed for the procession of the study with raw chicken specimens.

The raw chicken experiments had to be performed on the chicken knee joint as opposed to the chicken hip joint because testing on the chicken hip joint would involve buying a whole chicken, and the resources were not available for this type of experimentation at this time. For this reason, all experiments on the chicken specimens were performed on fresh raw chicken quarters with nuts attached to the articular surface of the tibia and the head of the femur. The preliminary data was obtained to observe whether repeatable data could be obtained across back-to-back and nonconsecutive sets of trials for an intact chicken knee. Fortunately, this was observed for the coherence, phase, and transfer function graphs across all trials. The next step

was inducing separation and dislocation into the chicken knee joint in order to simulate different degrees of dislocation in the infant hip joint. The intact knee was a little different, but the partially dislocated and foam separated knees all showed similar trends with slight differences in coherence, phase, and transfer function. The most interesting aspect of this experiment was the dramatic changes in all graphs in the case of complete dislocation as seen by the different transfer function pattern and the dips in coherence. The most interesting findings lied in the numerical differences in the transfer function values of different dislocation cases when compared to the intact chicken knee.

Experimental errors throughout the study were accounted for by the capturing of experimental setups before each nonconsecutive set was run. This was to ensure that there was no variation in data introduced by a setup that may have not been similar to the previous set. Accelerometer wax was weighed out each and every time it was placed on the nuts attaching the sensors to the bones, and the exciter and sensors were calibrated before the start of each experiment. However, confounding variables could have included issues with the wires used for the sensors or exciters, problems with the MATLAB DDH program, or even the loosening of components either on the 3D bone model or on the raw chicken itself.

Further experimentation would involve replicating more experiments when it comes to chicken knee dislocation and quantifying that variability as well. The goal is to see if the optimal frequency range of limited variability seen in the 3D printed bone model holds true for a soft tissue model like the raw chicken. In addition, with more resources, experimentation could begin on a whole chicken model so that the hip joint may be tested instead of the knee joint. Although the hip and knee joints of chickens and humans are both synovial, the hip joint's ball-and-socket

nature is different from the hinge joint structure of the knee. In the future, upon tweaking of the experimental techniques and narrowing of the optimal frequency to be used on the hip joint, the exciter and sensor system may be tested in a clinical setting with infants. Of course, this would first take place in patients with nondislocated hip joints, because the tool should not be used for diagnosis until it is certain that the data from the first human trials is repeatable. However, this is something to look forward to in the future.

LIST OF REFERENCES

Bickley, L. S., Szilagyi, P. G., Bates, B. (2009). *Bates' Guide to Physical Examination and History Taking* (Tenth ed.). Philadelphia, PA: Lippincott Williams & Wilkins.

Geswell, M., Sinha, N., Mandel, M., Wheatley, B., Mirenda, W., & Seeley, M. (2020). Improving resident education through unstable chicken hips: a novel way to teach an infant hip examination. *J Pediatr Orthop B*. doi:10.1097/BPB.0000000000000762

Harper, P., Joseph, B. M., Clarke, N. M. P., Herrera-Soto, J., Sankar, W. N., Schaeffer, E. K., . . . International Hip Dysplasia, I. (2020). Even Experts Can Be Fooled: Reliability of Clinical Examination for Diagnosing Hip Dislocations in Newborns. *J Pediatr Orthop, 40*(8), 408-412. doi:10.1097/BPO.0000000000001602

Hassan, T., McKinney, L., Sandler, R.H., Kassab, A., Price, C., Moslehy, F., & Mansy, H.A. (2018). An Acoustic Approach for Detection of Developmental Dysplasia of Hip. *2018 IEEE Signal Processing in Medicine and Biology Symposium (SPMB)*, 1-6. doi:10.1109/SPMB.2018.8615627

Kapicioglu, M. I., & Korkusuz, F. (2008). Diagnosis of developmental dislocation of the hip by sonospectrography. *Clin Orthop Relat Res, 466*(4), 802-808. doi:10.1007/s11999-008-0163-1

Kotlarsky, P., Haber, R., Bialik, V., & Eidelman, M. (2015). Developmental dysplasia of the hip: What has changed in the last 20 years? *World J Orthop, 6*(11), 886-901. doi:10.5312/wjo.v6.i11.886

Perez-Oliva, H., Cordova-Fraga, T., Padilla-Raygoza, N., Gomez-Aguilar, J. F., Baleanu, D., Sosa-Aquino, M., Bernal-Alvarado, J., & Guzman-Cabrera, R. (2016). Electroacoustic Device for Hip Dysplasia Assessment. *Revista de Chimie 67*.

Shaw, B. A., & Segal, L. S. (2016). Evaluation and Referral for Developmental Dysplasia of the Hip in Infants. *Pediatrics, 138*(6). doi:10.1542/peds.2016-3107

Yang, S., Zusman, N., Lieberman, E., & Goldstein, R. Y. (2019). Developmental Dysplasia of the Hip. *Pediatrics, 143*(1). doi:10.1542/peds.2018-1147